Water Vapour Climate Change Initiative (WV_cci) - CCI+ Phase 1

Climate Assessment Report (CAR)
Ref: D5.1
Date: 31 May 2022
Issue: 3.1
For: ESA / ECSAT
Ref: CCIWV.REP.018

This Page is Intentionally Blank

Project :	**Water Vapour Climate Change Initiative (WV_cci) - CCI+ Phase 1**
Document Title:	**Climate Assessment Report (CAR)**
Reference :	**D5.1**
Issued :	**31 May 2022**
Issue :	**3.1**
Client:	**ESA / ECSAT**
Author(s) :	Ulrike Falk (DWD), Marc Schröder (DWD), Hélène Brogniez (UVSQ), Jorge Eiras-Barca (U. Vigo), Luis Gimeno (U. Vigo), Jia He (UVSQ), Daan Hubert (BIRA-IASB), Jean-Christopher Lambert (BIRA-IASB), Rene Preusker (SE), Tim Trent (U. Leicester, NCEO), Michaela Hegglin (UoR)

Document Change Log

Issue/ Revision	Date	Comment
1.0	1 September 2020	Initial submission to ESA
1.1	3 November 2020	RIDs from ESA, RID responses and updates according to RID responses
2.0	8 April 2021	Second version, submitted to ESA for review This includes details of *anticipated* work due to the extended time schedule of the project
3.0	2 March 2022	Third version, submitted to ESA for review
3.1	31 May 2022	Updated version with implemented responses to RIDs from ESA

TABLE OF CONTENTS

INDEX OF TABLES

INDEX OF FIGURES

1. INTRODUCTION

1.1 Purpose

This Climate Assessment Report (CAR) complements the detailed Level-2/Level-3 validation and comparisons described in the ESA WV_cci Product Validation and Intercomparison Report (PVIR) (D5.1). The climate assessment efforts within the ESA WV_cci project focus on the analysis of the clear-sky bias, trend estimation, variability analysis at various scales, atmospheric moisture transport and comparison to CMIP6 data.

Results related to atmospheric moisture transport and comparisons to CMIP6 are extended summaries from submitted publications.

1.2 Scope

This document describes the climate assessment of the water vapour products by the ESA WV_cci project. The activities are an integral part of the international research on atmospheric water vapour.

Specific tasks include:

- Trend estimation applied to long-term data records
- Analysis of the compliance with theoretical expectation
- Analysis of atmospheric moisture transport
- Climate studies using data from CMIP6 and ERA5.

The overall scope of this document is to assess strengths and weaknesses in the ESA WV_cci climate data records, and their value to the climate users.

1.3 The ESA Water_Vapour_cci project

Water vapour is the single most important natural greenhouse gas in the atmosphere, thereby constraining the Earth's energy balance, and it is also a key component of the water cycle. Due to its importance, the WMO's Global Climate Observing System (GCOS) program has highlighted water vapour as an Essential Climate Variable (ECV) in the GCOS 2016 Implementation Plan (GCOS, 2016). There is consequently the need to consolidate our knowledge of natural variability and past changes in water vapour and to establish climate data records of both total column and vertically resolved water vapour for use in climate research. These climate data records need to be homogeneous in space and time, which bears great challenges due to changing instrument characteristics and performances. Well-characterised uncertainties are a key attribute of such climate data records in order to reduce the uncertainty in estimates of climate change and global radiative forcing.

The Climate Change Initiative (CCI) is a program of the European Space Agency (ESA), established to tackle the challenges encountered in merging climate data records of ECVs and has the goal to provide climate modellers and researchers with long-term satellite records from current and past European (and other space agencies') missions. The ESA CCI Water Vapour project generates stratospheric and tropospheric water vapour by developing novel methods to determine, merge and estimate such water vapour data and associated uncertainties.

1.4 The WV_cci datasets

The WV_cci datasets comprise four CDRs:

- CDR-1: gridded monthly and daily time series of TCWV in units of kg/m^2 that cover the global land areas with a spatial and temporal resolution of 0.05° and daily, respectively. It covers the period July 2002 to December 2017.
- CDR-2: gridded monthly and daily time series of TCWV in units of kg/m^2 that cover the global land and ocean areas with a spatial and temporal resolution of 0.05° / 0.5° and daily, respectively. It covers the period July 2002 to December 2017.
- CDR-3 contains the vertically resolved water vapour ECV in units of ppmv (volume mixing ratio; VMR) and will be provided as zonal monthly means on the SPARC Data Initiative latitude/pressure level grid (SPARC, 2017; Hegglin et al., 2014). It covers the vertical range between 250 hPa and 1 hPa, and the time period 1985 to the end of 2019.
- CDR-4 consists of three-dimensional vertically resolved monthly mean water vapour data (in ppmv) with spatial resolution of 100 km, covering the troposphere and lower stratosphere.

2. ANALYSIS OF THE CLEAR-SKY BIAS

Ulrike Falk (DWD), Marc Schröder (DWD), Rene Preusker (SE)

Total column water vapour can be retrieved from satellite observations on a global scale since the late 1970s. Measurements are obtained over land and ocean in different parts of the electromagnetic spectrum: among others, the ultraviolet/visible (UV/vis), infrared (IR), the microwave, and with high spatial resolution over land the near infrared (NIR) frequencies. Except for microwave observations, all related retrievals are predominantly applied under clear-sky conditions. Though instantaneous water vapour products show high quality and low uncertainty, this is not necessarily true for the gridded and temporally averaged products: Conditions in clouds are typically more humid than the surrounding clear-sky areas, and are not taken into account by the satellite's clear-sky observations. This effect is called clear-sky bias (CSB) and is in the order of 10% (Sohn and Bennartz, 2008). In order to provide a reliable uncertainty estimate for gridded and temporally averaged clear-sky products, the contribution of this source of uncertainty to the total uncertainty needs to be characterised.

2.1 Characterisation of the clear-sky bias using ERA5 data

Within the framework of the EU-funded Copernicus Climate Change Service (C3S), ECMWF produced the ERA5, i.e. the fifth generation of ERA reanalysis of the global weather and climate (Hersbach et al., 2020). The main objective of the ERA5 project is to give a detailed record of the global atmosphere, land surface and ocean waves from 1950 onwards. The ERA5 data is being used to look into the differences between full (all-sky) TCWV data and TCWV data filtered by the obstruction by cloud occurrence. Data records and access are described in full detail in the DARD (2021).

All metrics are described in the PVP (2021), but for the sake of completeness, the detailed formulas are given here. One major main difference between the ERA5 data output and the satellite observations is the time stamp of the single data- and grid points. The L3 globally gridded satellite datasets consist of daily and monthly averages where each grid point contains satellite observations from a specific overpass time. Each satellite observation is strictly speaking a function of local time (LT). However, the NIR sensors taken into account in the WV_cci are on platforms that are in sun-synchronous orbit, meaning that the satellites are crossing the equator and any point on the Earth’s surface at approximately the same local time. Deviations may occur from eccentricity. However, this approximation is valid at near-nadir pixels in view of the considered hourly time window (see below). The ERA5 data, on the other hand, are datasets of model output for each time step of the model run in UTC. Here, the globally gridded data fields have the same time stamp in UTC for each time step of the model output. In order to compare observations with model data, it is, thus, imperative to convert the data fields into the same temporal systems. This is done here by slicing the ERA5 data into longitudinal fields according to local time of the respective satellite overpasses and patch them back into data fields with the same local time stamp (e.g. MERIS overpass local time ≈ 10 am) with a temporal resolution of 1 hour translating into 15° spatial resolution. The temporal collocation window is then set to ±0.5 hours. Note that the fixed swath width in km covers increasingly larger longitude regions with increasing latitude. In consequence, the swath can cover more than one hourly bin. This effect is ignored in our analysis, i.e. ERA5 are not exactly sampled as a single, specific satellite would have seen it. Instead, the results are meant to allow for a general analysis of and potential application to various satellites. Also, the CSB can be analysed at e.g. 10 and 11 local time to see an impact of differences in temporal sampling.

The cloud mask is simulated by filtering total column cloud liquid water (TCLW) and total cloud cover (TCC) of ERA5. The filters were set to TCC > 0.95 and TCLW > 0.005 kg m^{-2} following the work of Sohn and Bennartz (2008). The filter criteria were responsible for the exclusion of 75% of the data points per month on average, with an annual cycle of average amplitude of approximately 7.5% and very little year-to-year variability. Of the filtered data, the TCC criterion filtered 66.3% ± 0.3%, and the TCLW criterion 87.1% ± 0.2% of all filtered data. It is noted that Stubenrauch et al. (2012) observe 62 and 69% of average global cover in two different MODIS products.

2.1.1 Tools

The clear-sky bias (*CSB*) is estimated here as the difference of the sampled data to the climatology (see PVP, 2021), applied to each grid point:

$$CSB_{i,j}(t) = x_{i,j}(t) - \overline{C_{i,j}}^{(2002-2012)}$$

where *i* is latitude, and *j* is the longitude, $\overline{C_{i,j}}^{(2002-2012)}$ the all-sky and all times climatology computed over the whole time period (here 2002–2012) for each grid point, and t is the time step (e.g. equator crossing time of 10 am local time).

We dissect the *csb* into its local time scale, monthly and spatial components, i.e. *CSB* = *function*(local time, month, longitude, latitude):

$$\overline{CSB_{i,j}}^{T} = \overline{\left(x_{i,j}(t) - \overline{C_{i,j}}^{(2002-2012)}\right)}^{T}$$

where *T* indicates an average at each equator crossing time (here all full hours), at each month over all years. The respective standard deviation is given as uncertainty measure for each time scale. The results are plotted spatially and assessed qualitatively (see Section 2.1.2).

2.1.2 Results of ERA5 analysis

The climatology of the CSB calculated from the hourly ERA5 climate data records is displayed in Figure 2-1. It shows a coincidence of maximum clear-sky biases with cloud occurrence, i.e. over the ITCZ and extratropical storm tracks, and of minimum and even positive clear-sky bias over deserts and stratocumulus regions. As mentioned in the introduction of Section 2 it is expected that the clear-sky bias is generally negative as observed for most regions and as seen in an average CSB of -0.85 kg/m^2. However, also positive values are observed with a similar spatial structure as in Sohn and Bennartz (2008). Over ocean such regions mainly occur in the presence of stratocumulus clouds. In the presence of such clouds, mostly dry atmospheres are observed, while in clear sky the atmosphere likely exhibits more mixing and is thus more humid (Fetzer et al., 2006; Sohn and Bennartz, 2008).

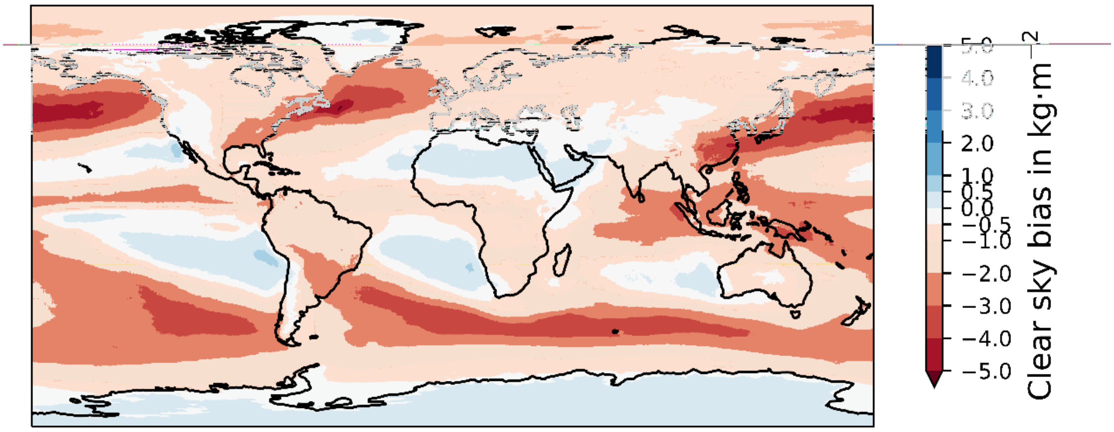

Figure 2-1: 11-year climatology of the clear-sky bias assessed for ERA5 data records on hourly basis (time period 2002–2011), resulting in an area-weighted global CSB_{mean} = -0.85 kg m^{-2}.

According to the spatial location, the filters of the CSB assessment lead to a reduction in data points used for averaging over the 11-year time period.

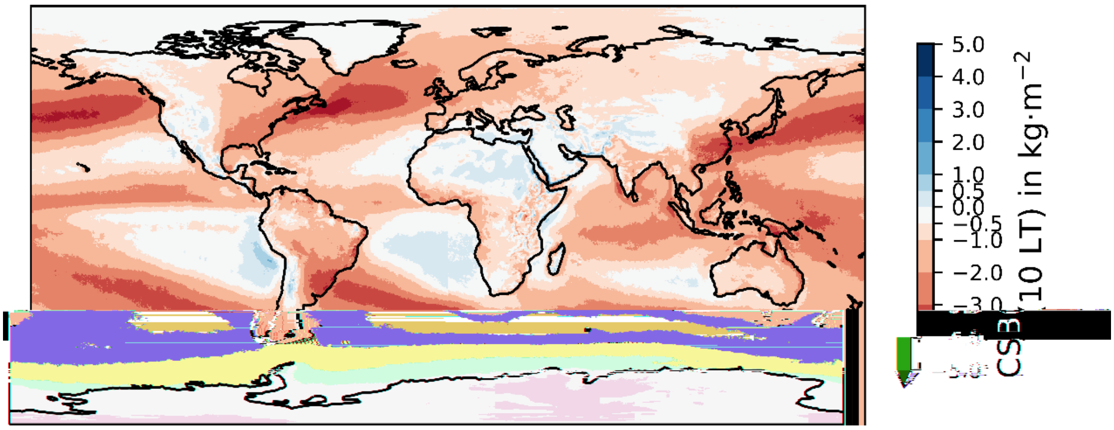

Figure 2-2: 11-year climatology of the clear-sky bias for local time, LT=10; the assessment is based on hourly ERA5 data records for local overpass time of MERIS (time period 2002–2011). The area-weighted global average computes to CSB_{mean} = -0.87 kg m^{-2}.

Figure 2-2 shows the climatological clear-sky bias for 10:00 local time. Overall the two climatologies (Figure 2-1 and Figure 2-2) exhibit similar features, except that the latter seems to be damped somewhat and more noisy. Theoretically, the differences between the two climatologies (Figure 2-1 and Figure 2-2) illustrate the effect of the temporal sampling bias in the clear-sky bias, which is related to the overpass time of the satellite. It seemingly results in a more noisy pattern especially over tropical and subtropical land surfaces over South America and Africa. Also visible in the comparison is the less intense wet bias in the northern mid to high latitudes over sea surfaces. The reduction of the dry bias for the Antarctic continent is only in the order of 0.5 kg m^{-2}. Since observations for this region are scarce, and modelling efforts still carry high uncertainties, this might also be considered artificial.

The monthly climatologies of the CSB are displayed in Figure 2-3. It illustrates the impact of the large-scale circulation pattern like the movement of the ITCZ and an intensification of the wet bias for ocean surfaces in mid to high latitudes during the summer months of the respective hemisphere.

Figure 2-4 shows an example of the hourly CSB assessment for the month of January for the Amazon region to demonstrate the diurnal scale of the CSB for tropical regions. Here, the diurnal course in, especially, cloud coverage is dominating the seasonal course. White spots signify areas with no data due to the cloud mask filter in the CSB assessment. The Amazon basin shows a regular development of (convective) cloud coverage that is associated with the diurnal course of solar incidental radiation. Over the year, this region shifts slightly south and north according to the position of the ITCZ.

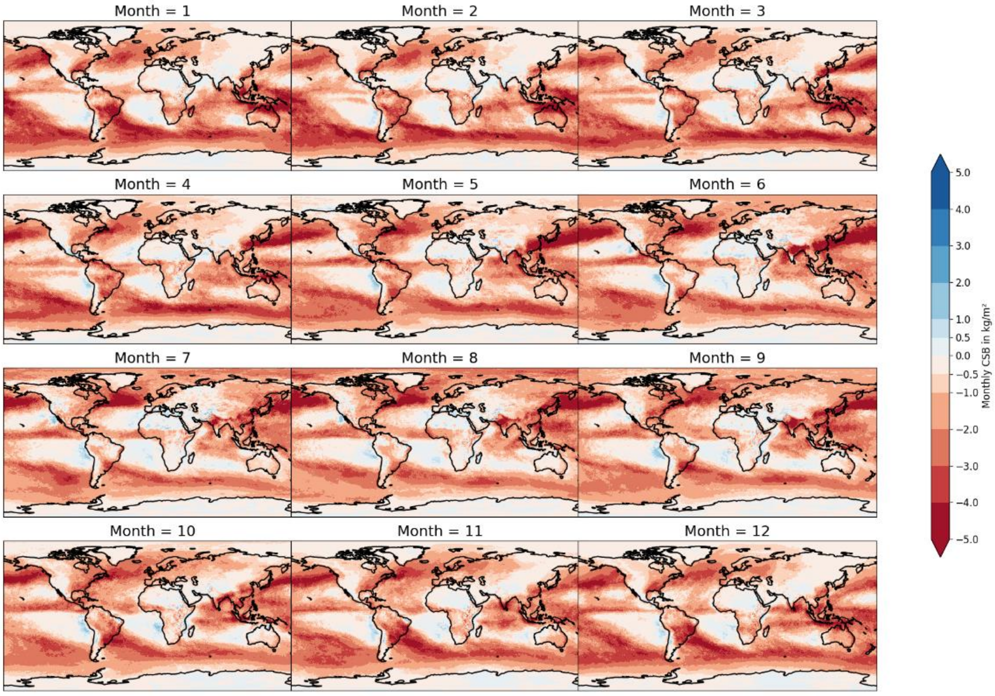

Figure 2-3: Monthly assessment of the clear-sky bias assessment for ERA5 data records for the time period 2002–2011.

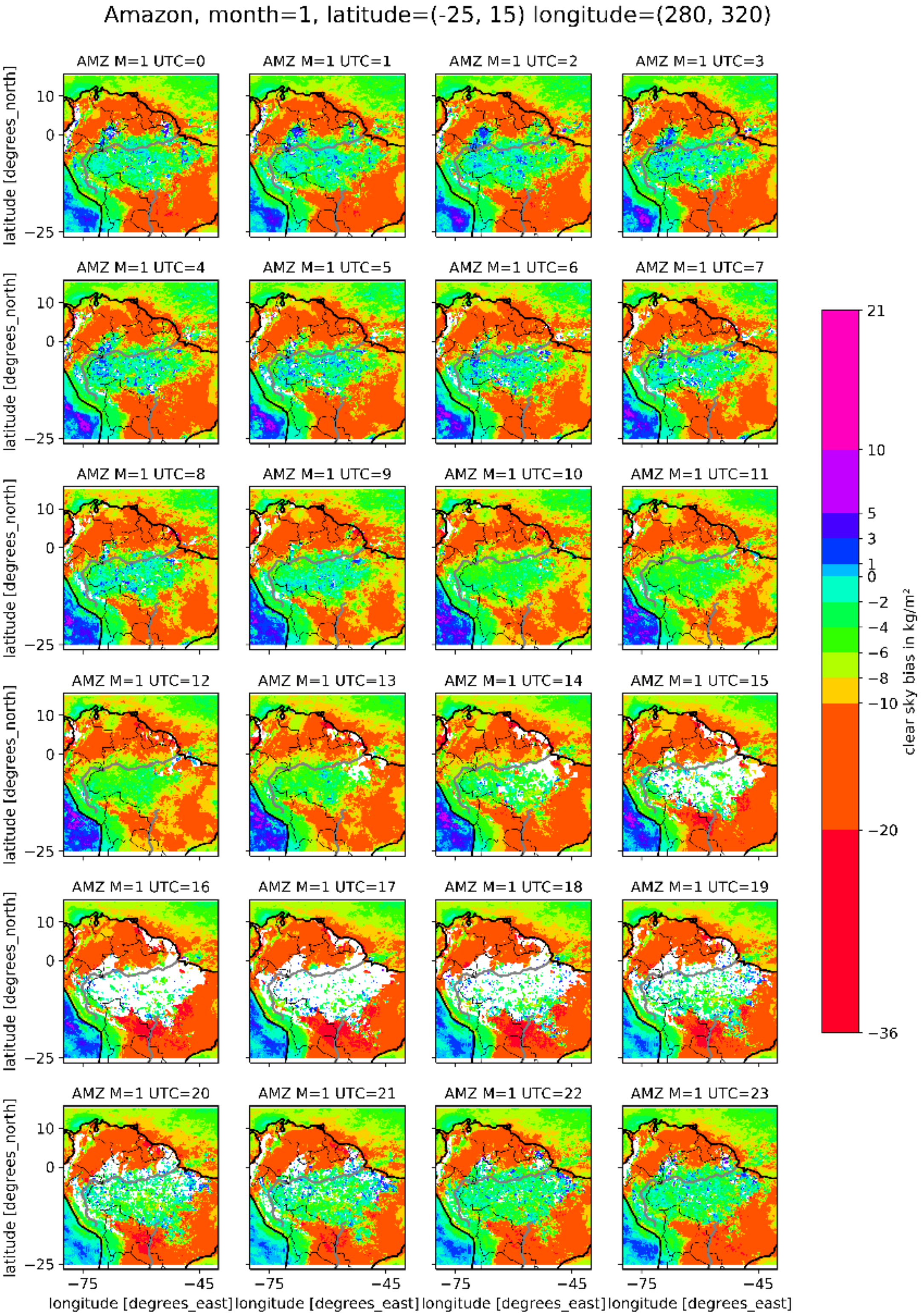

Figure 2-4: Example of hourly assessment of the clear-sky bias assessment for the Amazon region based on ERA5 data records for January (month = 1) and the time period 2002–2011. White areas mean no data is available.

2.2 Validation of clear-sky bias assessment

For the validation of the CSB assessment on the basis of ERA5 data records, two different cloud masks were used to filter GPS data from the SuomiNet global observation network. Data records and access are described in full detail in the DARD (2021).

The validation of the CSB analysis was carried out for two time periods: 2005–2011 (MERIS cloud mask) and 2016–2018 (OLCI cloud mask). The restraining element of the time periods is the existence of a valid cloud mask. The calculated statistics for the two assessments both show a significant correlation between the ERA5-based estimation of the CSB, and a mean non-zero bias of the CSB. The data has been filtered for GPS stations and ERA5 data at the same point showing a normal distribution, in other words, if the data time series can be considered representative for that specific location. We attribute failure to comply with the restrictive condition of normal distribution to, firstly, non-representativeness of the GPS observations (a possible error source is also the assumption of a tropospheric temperature within the signal-processing). Secondly, the cloud mask is associated with a lot of problems in, especially, coastal areas, and, thirdly, the regional circulation and climatologies might show systematic bias towards non-normal distributed observations.

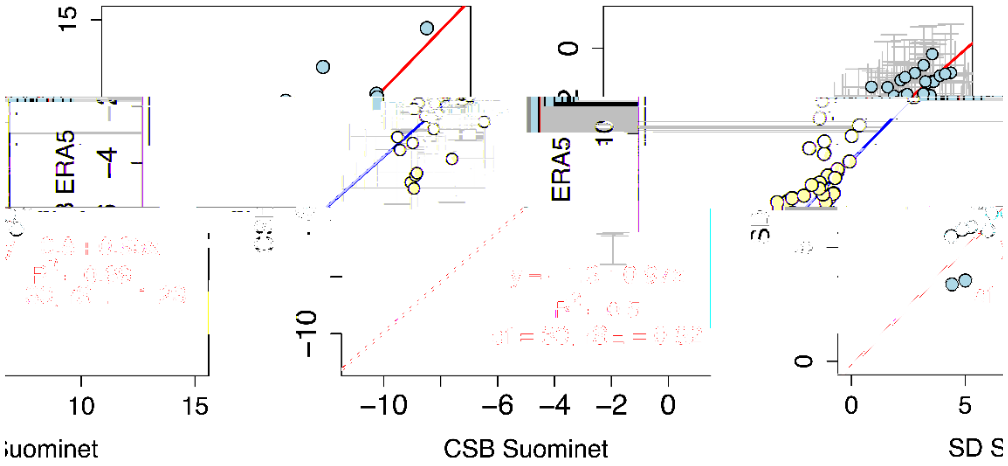

Figure 2-5: Validation of the clear-sky bias assessment: standard deviation (SD) and CSB in kg m^{-2} calculated from ERA5 data records against SD and CSB in kg m^{-2} derived from analysis of GNSS (Suomi Net) data records using the MERIS cloud mask for the time period 2005–2011. Error bars are derived from uncertainties attached to the observations.

The statistics using the MERIS cloud mask (time period 2005–2011) yield a rather good correlation with an R^2 = 0.5 for a sample size of N = 30, whereas the statistics for the

OLCI cloud mask result in a much higher $R^2 = 0.82$, but for a smaller sample size of $N = 12$. The mean difference in *CSB* between ERA5 and SuomiNet is 3.65 kg m^{-2} when using the MERIS cloud mask for the time period 2005–2011, and is -1.13 kg m^{-2} when using the OLCI cloud mask for the time period 2016–2018. The larger sample size of the *CSB* assessment (*df*=30) for the time period 2005–2011 using the MERIS cloud mask yields a normal distribution of the differences between the clear-sky biases, whereas the sample size for the time period 2016–2018 using OLCI cloud mask amounts to only *df*=12. The error bars (in Figure 2-5 and Figure 2-6) are derived from the error propagation of uncertainties attached to the data records. In both figures it is evident that the ratio of standard deviation to the calculated CSB is for most data points around or greater than one, and at least greater than 0.25. For both validation efforts, a higher sample size would thus be necessary to deduce statistically reliable results.

The extreme values for the CSB assessment do not fall below $CSB_{era5,\ min} > -6$ kg m^{-2} and $CSB_{suo,\ min} > -4$ kg m^{-2}, whereas in the OLCI CSB assessment, more extreme values, $CSB_{era5,\ min} < -10$ kg m^{-2} and $CSB_{suo,\ min} < -7$ kg m^{-2} are visible.

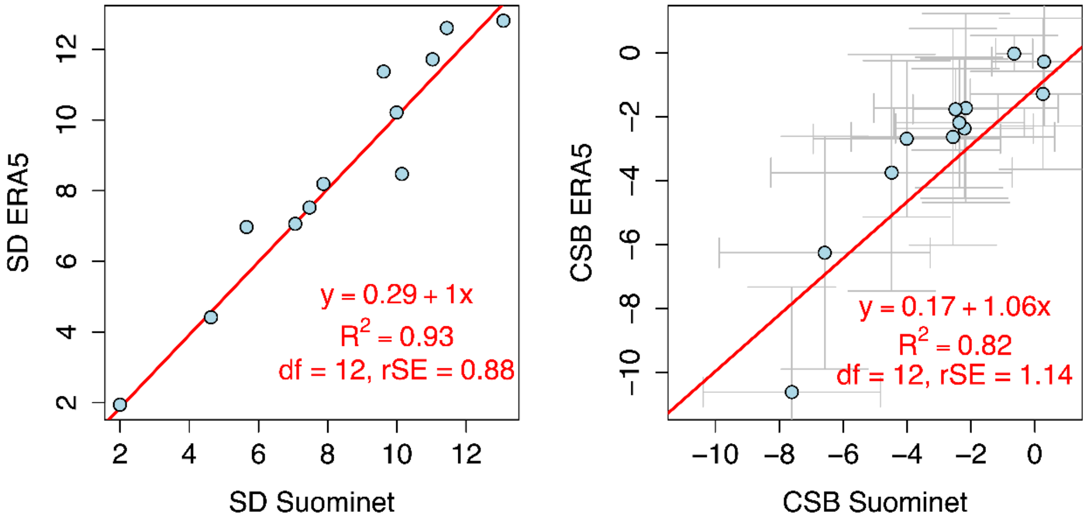

Figure 2-6: Validation of the clear-sky bias assessment: standard deviation (SD) and CSB in kg m^{-2} calculated from ERA5 data records against SD and CSB in kg m^{-2} derived from analysis of GNSS (SuomiNet) data records using the OLCI cloud mask for the time period 2016–2018. Error bars are derived from errors attached to the observations.

2.3 Significance of clear-sky bias assessment

The significance of the CSB assessment is tested by analysing the ratio of the standard deviation of the time series against the value of the CSB. The natural variability on the diurnal and monthly scale leads to high standard deviations of the time series, and thus, a ratio of SD to CSB that can be close to or greater than 1 kg m^{-2}.

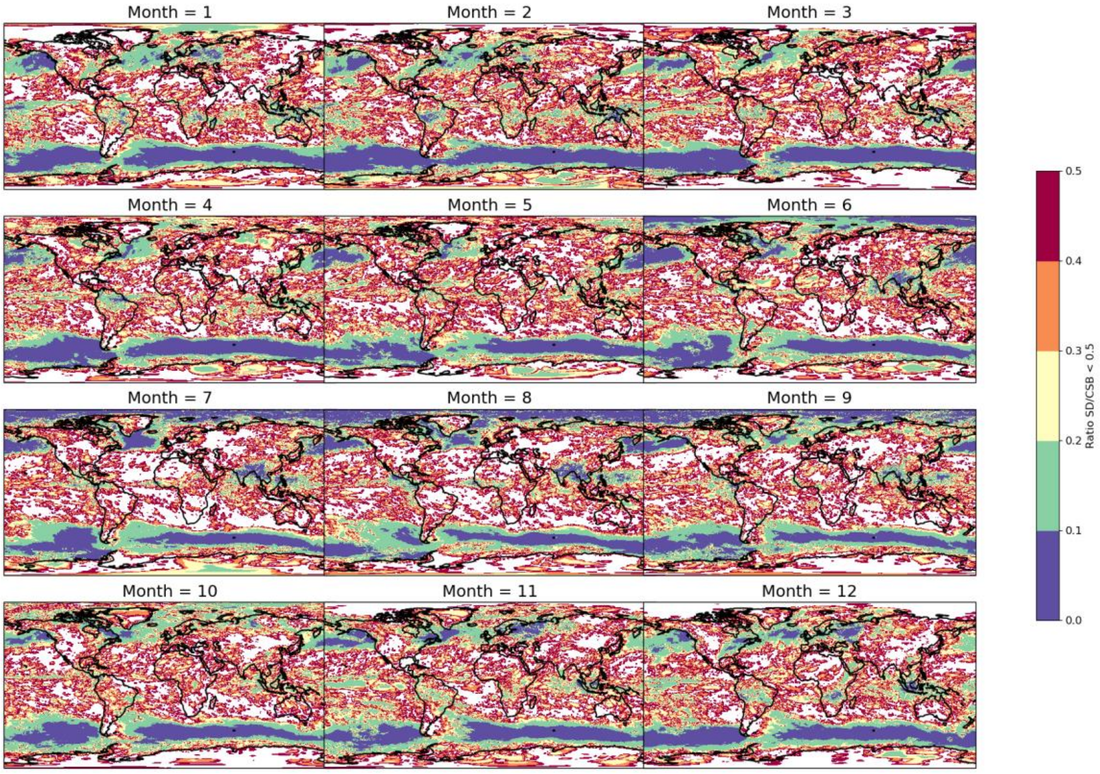

Figure 2-7: Ratio of standard deviation (SD) to clear-sky bias (CSB) with *SD/CSB* < 0.5 based on monthly CSB assessment from ERA5 data records for the time period 2002–2012. In white are points with a ratio *SD/CSB* ≥ 0.5.

Shown in Figure 2-7 is the global distribution of the ratio of the monthly climatologies of standard deviation (SD) of the clear sky bias to the monthly climatologies of CSB, filtered for values *SD/CSB* < 0.5. Most regions in the latitudes below ±45° exhibit a heterogeneous pattern of mostly red areas, i.e. *SD/CSB* ≥ 0.4, and white areas, i.e. values *SD/CSB* ≥ 0.5. The CSB assessment for most of these tropical and subtropical latitudes is thus considered as non-significant or just significant. In comparison to the monthly CSB climatologies (see Figure 2-3), it is apparent that regions with higher values for the CSB also coincide with higher values of SD. For areas above 45° South and North, the calculated clear-sky bias leaves mostly sub-polar and polar regions marked in green and blue, meaning a significant CSB assessment. This is caused by the lower standard deviation of the grid-point time series that can be attributed to the low sample sizes due to the cloud filter in the CSB assessment, though. The distribution for the northern summer months shows a slightly better adherence to this restriction. Due to the high natural variability in the time series of CSB assessment, longer time series are necessary.

The CSB is either non-significant or hardly significant and elsewhere affected by a low number of valid points. Thus, it is proposed not to include the clear-sky bias in the CDR-1 and CDR-2 NIR data, but to make the user aware of the existence and magnitude of the CSB effect in the Product User Guide (PUG, 2021).

2.4 Conclusions

The CSB assessment based on the analysis of ERA5 data records shows the high natural variability in the time series of CSB and indirectly cloud coverage (cloud fraction). Climatologies of CSB on annual and monthly scale show a distinct spatial distribution of wet and dry biases that are dominated by large-scale circulations for the mid to high latitudes and by the diurnal course of cloud coverage and the position of the ITCZ in tropical and subtropical regions.

The area-weighted global average of the CSB is calculated to $CSB_{\mathrm{mean}} = -0.85$ kg m^{-2} for the full-day assessment, and to a slightly lower $CSB_{\mathrm{mean}} = -0.87$ kg m^{-2} for the assessment based on local time LT=10.

For latitudes within the range of approximately ±45°, the CSB assessment can be considered not significant or just about significant. For the higher latitudes the CSB assessment can be considered significant according to the criterion of $SD/CSB < 0.5$, but sample sizes are rather low. It is therefore recommended to carry out the CSB assessment and validation on longer time series.

Thus, and in order to further assess its usefulness, it is recommended to include the CSB in the analysis of consistency of the CDRs as a sanity check and not to include the CSB in the CDRs themselves.

3. ANALYSIS OF VARIABILITY, TRENDS AND COMPLIANCE WITH THEORETICAL EXPECTATION USING WV_CCI TCWV DATASETS (CDR-1, CDR-2)

Ulrike Falk (DWD), Marc Schröder (DWD), Tim Trent (U Leicester, NCEO)

A focus of this section is on the analysis of global trends in TCWV using WV_cci CDR datasets. This analysis not only provides these estimates for comparison but the trend analysis needs to be understood as a tool to potentially identify issues in the datasets, very similar to approaches in the GEWEX Water Vapor Assessment (G-VAP, see, e.g. Schröder et al., 2017, 2018, 2019). TCWV trends are assessed on a global scale, i.e. by providing estimates on grid basis as spatial maps and by analysing near global averages. During trend estimation the Niño 3.4 El Niño Southern Oscillation (ENSO) Index and four frequencies in order to address the annual cycle are fitted as well. The variability is shown as spatial maps of associated weights.

Furthermore, the compliance of variability in TCWV with theoretical expectation using ESA SST_cci and ESA LST_cci data records is assessed. In view of increasing temperatures it can be expected that TCWV will increase at a rate of approximately 6 – 7.5 %/K according to the Clausius–Clapeyron law.

Associated results are put into the perspective of G-VAP results and results available from the literature.

3.1 Datasets

The CM SAF / WV_cci TCWV product consists of microwave-based observations over the ice-free ocean from the Hamburg Ocean Atmosphere Parameters and Fluxes from Satellite data (HOAPS) and of near-infrared based observations over land, sea-ice and coasts. The combined global TCWV dataset covers the period August 2002 until December 2017 and is provided as monthly and daily means with a spatial resolution of 0.05° and 0.5°. It is noted here that CDR-2 is released by European Organisation for the Exploitation of Meteorological Satellites (EUMETSAT) Satellite Application Facility on Climate Monitoring (CM SAF) (https://doi.org/10.5676/EUM_SAF_CM/COMBI/V001). As CDR-1, the WV_cci TCWV dataset over land, is fully included in CDR-2 without changes by any means, we analyse CDR-2 "only". Subsequently we speak of CDR-1 if land only TCWV values are meant; else we use the term CDR-2. Further details on CDR-1 and CDR-2 are given in the PSD v3.2.

Validation results carried out within WV_cci show that bias and cRMSD exhibit a different level when OLCI data is included into the CDRs (PVIR v2.1). Although this is still within user requirements, it would create a break point and thus impact any trend analysis in a non-physical way. The MERIS and MODIS period is stable when analysing clear-sky and 10 am local time averages over global land surfaces. Thus, we use the MERIS and MODIS time series only, i.e. the period until March 2016.

The trend, compliance and variability analysis is also carried out for AIRS+AMSU v6 and ERA5. Both data records exhibit global coverage. AIRS contains monthly means only and is provided at 1°x1° spatial resolution while ERA5 is also available at higher resolutions (see DARD v3.2 for more details).

In order to assess compliance with theoretical expectations following Clausius–Clapeyron, surface temperature data records from ESA SST_cci and from ESA LST_cci are used (see DARD v3.2 for more details). Both datasets characterise the surface while strictly speaking the air temperature at surface (TAS) should be used. Such a product was generated and provided by the EU-funded project EUSTACE (EU Surface Temperature for All Corners of Earth). Here, the dataset is called EUSTACE for simplicity and further details are given in the DARD v3.2. Note that the coverage of EUSTACE over ocean contains hardly any valid values after 2012. When analysing the anomaly time series of TAS and TCWV over land and ocean, the expected overall synchronisation in temporal variability is hardly visible after approximately 2014, maybe earlier over ocean. A clear identification of the exact date is hampered by low frequency variability (not shown). Thus, it was concluded, that the EUSTACE dataset is not used in this analysis. While an analysis over ocean using surface temperature is in most cases acceptable, an analysis over land is fairly strongly hampered by large differences between surface temperature and TAS, depending on region and time of day. Thus, the compliance over land is only analysed for CDR-1 and LST_cci data record. Further discussions are provided in Section 3.3.

3.2 Methodology

For a straightforward intercomparison of the results from trend analysis of between CDR-2, ERA5 and AIRS+AMSU, the analysis is carried out on the lowest common spatial resolution (here 1° x 1°) using monthly data, and over the common time period from 2002 to 2016. As a further requirement, commonly defined values are analysed only, i.e., where there are, for all time steps and in all data records, defined TCWV values. As a consequence from WV_cci internal analysis it was recommended to apply a common, conservative cloud mask prior to the estimation of near global averages and subsequent trend estimation. The reason is that the cloud masks between MERIS/OLCI and MODIS exhibit differences, such that in the case of MODIS significantly more valid values remain in the extra-tropics in monthly means which would lead to smaller global mean TCWV values relative to a global mean based on less contributions from the extra-tropics (see PVIR v2.1). The above approach indirectly ensures that this is not impacting the results related to analysis of (near) global averages.

Trend estimates are computed for TCWV averages over global, global land and global ice-free ocean surfaces and on grid-basis. In each case the trend estimation and estimation of associated uncertainties and their significance follows methodologies described in Weatherhead et al. (1998), Mieruch et al. (2014) and Schröder et al. (2016, 2019), similar to approaches applied in G-VAP. A linear regression is fitted to the time series simultaneously with the Niño 3.4 ENSO Index and four frequencies that allow for an analysis of annual cycles. The weights associated with ENSO and the annual cycle are discussed in the assessment of variability. The estimation of uncertainties also considers auto-correlation.

Finally, it is assessed whether or not changes in TCWV agree with change in surface temperature, i.e. as expected from Clausius–Clapeyron. Again, the methodology follows approaches used within G-VAP (Dessler and Davis, 2010; Mears et al., 2007; Schröder et al., 2016, 2019). Deseasonalised anomalies of TCWV and surface temperature are filtered with a 12-month low-pass filter to smooth the time series. Subsequently the linear regression between deseasonalised and smoothed anomalies of TCWV and surface temperature is computed.

3.3 Results

3.3.1 Variability

The variability in TCWV associated with ENSO and annual cycles is described and inter-compared by showing global maps of weights which are output from trend estimation (see Section 3.2) and by considering CDR-2, ERA5 and AIRS+AMSU.

Spatial maps of the annual cycle contribution to variability in TCWV for the three data records are shown in Figure 3-1. Large (small) absolute weights indicate the presence of a strong (small) annual cycle. Weights in the Southern Hemisphere are actually negative which reflects the shift by half a year between boreal and austral summer in presence of a symmetric annual cycle. Generally, the strength of the annual cycle is stronger in the Northern Hemisphere than in the Southern Hemisphere and small annual cycles are present in the ITCZ, i.e. where the maximum northern and southern position of the ITCZ overlap, over parts of ocean deserts and the Southern Ocean. Peak values are usually associated with the movement of the ITCZ, here, its northern- and southern-most branches, monsoon activity, e.g. over India (see, e.g. https://www.clivar.org/clivar-panels/monsoons for a map of monsoon regions) and with low-level jet activity in boreal/austral summer (Gimeno et al., 2016), partly associated with Hurricane seasons (Yang et al., 2021). Interesting to see is the overlap of winter monsoon regions with minima in annual cycle weights. A local maximum in the weight of the annual cycle is observed off the coast of California in ERA5, CDR-2 and, less pronounced, in AIRS. Annual cycles in TCWV are observed over stratocumulus regions including the stratocumulus region off the coast of California (Millán et al., 2019). However, such annual cycles are also observed over the other stratocumulus regions (Millán et al., 2019) which do not exhibit peak values in the annual cycle weight.

Fairly good agreement between the three data records is observed. Differences in the annual cycle strength between ERA5 and CDR-2 are very small and most evident over the North of Australia and Brazil. Larger, but still small differences occur between AIRS and ERA5/CDR-2, with the strength of the annual cycle being generally weaker in AIRS.

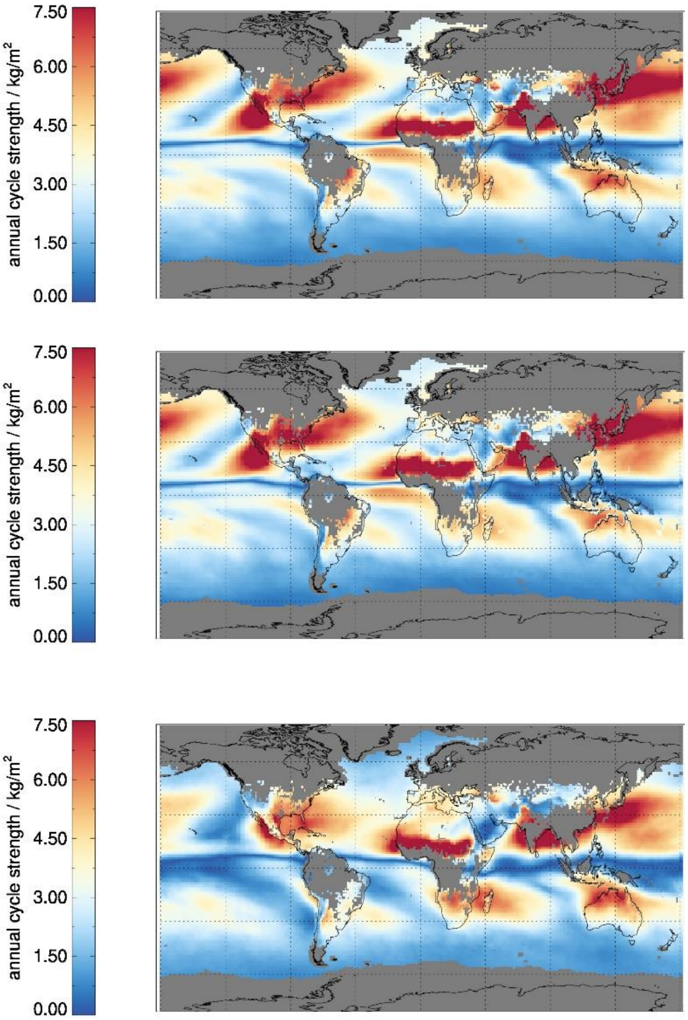

Figure 3-1: Maps of the annual cycle contribution to variability in TCWV for (top) ERA5, (middle) CDR-2 and (bottom) AIRS+AMSU. In order to increase readability the absolute values of the weight are plotted, i.e. weights in the Southern Hemisphere are actually negative.

Spatial maps of the ENSO contribution to variability in TCWV for the three data records are shown in Figure 3-2. Absolute large (small) weights indicate a strong (small) impact on variability by ENSO. Large positive weights would indicate an increase in TCWV with El Niño (or a decrease with La Niña) while large negative weights indicate an increase in TCWV with La Niña (or a decrease with El Niño). The observed spatial pattern is similar to features in similar analysis (e.g., Trenberth et al., 2005) and exhibits overlap with structures observed in changes in precipitation and SST with ENSO. Maximum values are observed in the central Pacific and minima are observed over the Western Pacific warm pool and the Southern Pacific Convergence Zone (SPCZ). A side maximum occurs over central West Africa and the Eastern Indian Ocean. A few smaller positive weights can be observed which are likely linked to ENSO teleconnections (e.g. Yeh et al., 2018).

Hardly any differences between CDR-2, AIRS+AMSU and ERA5 can be observed in the ENSO contribution to variability in TCWV.

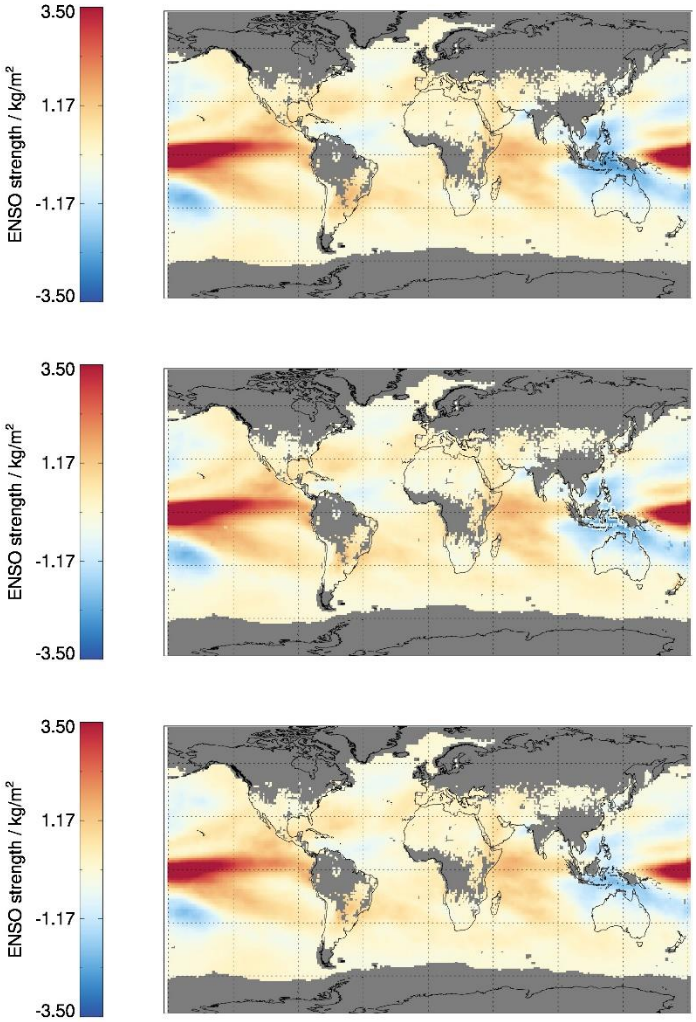

Figure 3-2: Maps of the ENSO contribution to variability in TCWV for (top) ERA5, (middle) CDR-2 and (bottom) AIRS+AMSU.

3.3.2 Trends

In this subsection the trend estimates of TCWV are analysed using CDR-1, CDR-2, AIRS+AMSU and ERA5 data. Trends and their uncertainty are estimated as described in Section 3.2. An analysis of large-scale averages is followed by a presentation of spatial maps.

Figure 3-3 shows the anomaly time series of TCWV over global, global land and global ice-free ocean surfaces for all three data records. Results from linear regression are plotted as straight lines and the associated slope, i.e. the trend estimate together with the associated uncertainty is given in the legend. The La Niña and El Niño events are visible as minima (2008) and maxima (2010, 2016) in all the time series, with the maximum value in 2016 being the absolute strongest anomaly in all time series.

The time series are very similar between the three data records. Maximum (but small) differences in anomalies are associated with ENSO over global ice-free ocean. It is noted that the combined results from global land and global ocean are not necessarily matching results shown in the global time series because the latter also includes sea-ice and coastal regions as well as large inland water bodies. These regions exhibited reduced quality during validation (see PVIR v2.1). While AIRS+AMSU and ERA5 exhibit fairly similar trend estimates, the CDR-1 and CDR-2 trends are larger in the three considered cases. Over ocean this difference is smallest but still significant given the associated uncertainties.

The observed trend estimates should not be considered as an analysis of climate change, mainly because the considered temporal coverage is fairly short but also because the trend estimates are strongly affected by the El Niño event at the end of the time series. When looking at Figure 3-3 it is obvious that trend estimates would be significantly smaller when the period until 2015 would be considered only. The presence of an El Niño event in temporal vicinity of the start of the considered period was analysed in Mieruch et al. (2014) and a change in trend estimates by a factor of approximately 2 was observed when changing the start data from 1991 to 1997. The importance of such an impact can obviously be generalised to the presence of an ENSO event relative to the start and/or stop of the considered period. Other trend estimates are given in, e.g. Sherwood et al. (2010), Mieruch et al. (2014), and Schröder et al. (2016, 2017). However, due to differences in considered periods but also due to differences in the considered spatial extend the results can hardly be compared. Nonetheless, we note that, not surprisingly, the trends given here are usually larger than trends given in the literature.

It is mentioned above that variability caused by ENSO is evident in the time series shown in Figure 3-3. The ENSO variability has a strong impact on trend estimates, even when the ENSO signal is fitted during trend estimation (this report; Mieruch et al., 2014). Certainly such a fit is not perfect but it should also be kept in mind there is a lag of approximately 2–3 months between the ENSO index (defined via SST) and the global mean response in air temperature and water vapour (Wentz and Schabel, 2000; Shi et al., 2018). Shi et al. (2018) also analysed this lag as a function of ocean basin and observed lags ranging from 0 months (Pacific) to 5–6 months (Indian Ocean). A global or regional lag is not considered during trend estimation and thus, given the lag, ENSO variability is not fully removed.

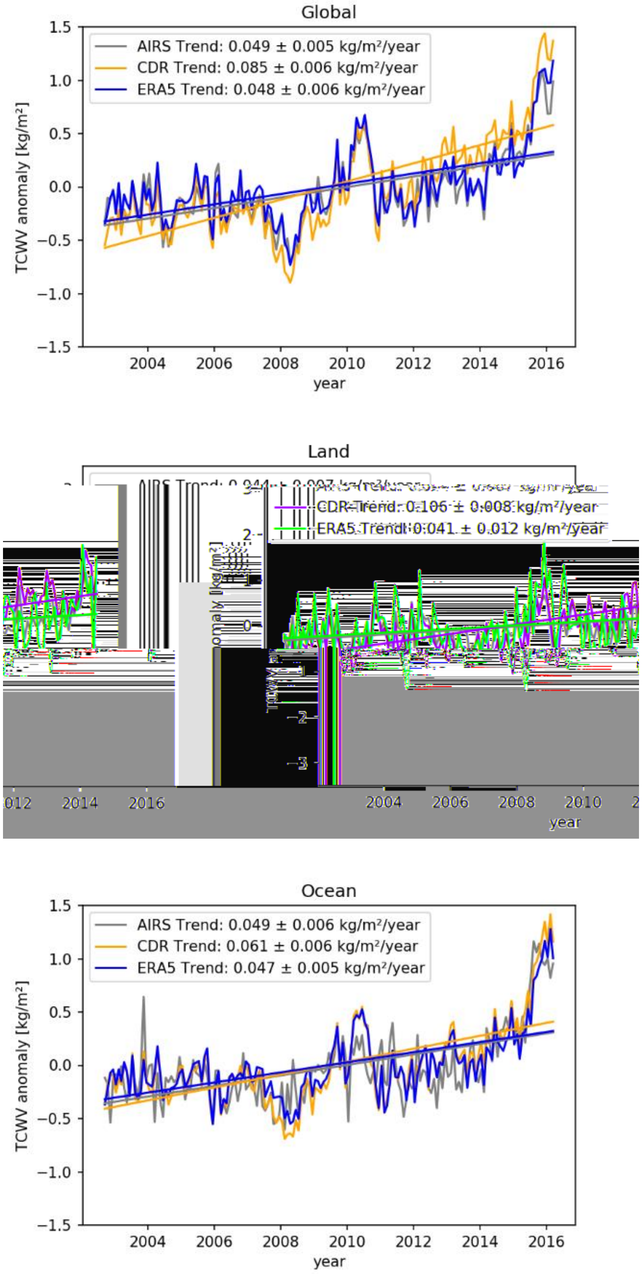

Figure 3-3: Time series of TCWV anomalies of (top) global, (middle) land, and (bottom) ice-free ocean data from CDR-1 (land), CDR-2 (else), AIRS+AMSU and ERA5 data. The plot covers the time period September 2002 – March 2016.

Global maps of trend estimates in kg/(m^2 decade) for ERA5, CDR-2 and AIRS+AMSU are shown in Figure 3-4. The uncertainty related to the trend estimates is shown in Figure 3-5. Figure 3-4 also shows the 95% confidence level. This level depends on uncertainty and trend strength, and trend estimates values associated with coverage probabilities larger than the 95% confidence level contours are considered to be significantly different from 0 kg/(m^2 yr). The trend estimates display a heterogeneous pattern of positive and negative trends. The largest positive trends are observed over southern regions of the Pacific tropical warm pool and regions south of it and the central Eastern Pacific. Largest negative trends are seen over the central Western Pacific and the SPCZ. Some smaller positive trend estimates seem to occur in regions with frequent cloud and rain presence. Regions with significant trend estimates are fairly small and mainly occur in regions with large absolute trend estimates, i.e. in the central Eastern Pacific and south of the Pacific tropical warm pool. The main exceptions are trend estimates in the Southeastern Pacific. This occurs in regions where the uncertainty estimates are fairly small while trend estimates are not maximal but still large. Trend estimates over land are hardly significant, despite the usually fairly small uncertainties. Thus, this relates to the presence of generally small trend estimates. It needs to be kept in mind that the significance level also depends on the number of valid observations, and the considered time period covers less than 14 years. The number of years required to allow climate change detection is discussed in Weatherhead et al. (1998) and Whiteman et al. (2011) and depends on the trend, the noise level and autocorrelation. Our results indicate that the estimation of significant trends on global scale would require longer time series.

The trend estimates, the coverage probability and the uncertainties are very similar between all three data records in terms of spatial structure and absolute strength. Largest and smallest, in a relative sense, absolute trends and uncertainties are observed for HOAPS and AIRS+AMSU, respectively, with a corresponding consistent picture in the coverage probability. However, it is recalled that CDR-2 exhibits reduced quality over coastal and sea-ice regions as well as over large inland water bodies (PVIR v2.1). This becomes evident here as well: large trends and large uncertainties are observed over coastal areas in CDR-2 and trend estimates appear different in CDR-1 over Lake Victoria and the Caspian Sea relative to ERA5 and AIRS+AMSU.

Again, a direct comparison to results published in the literature is hardly possible, given mainly the differences in considered periods. Nonetheless, it is noted that the spatial structure of observed trends exhibits differences relative to results shown in Schröder et al. (2016) and, to a lesser extent, to results shown in Trenberth et al. (2005). For completeness the considered periods are recalled here: 2002–2016 (this study), 1988–2008 (Schröder et al., 2016), and 1988–2001 (Trenberth et al., 2005).

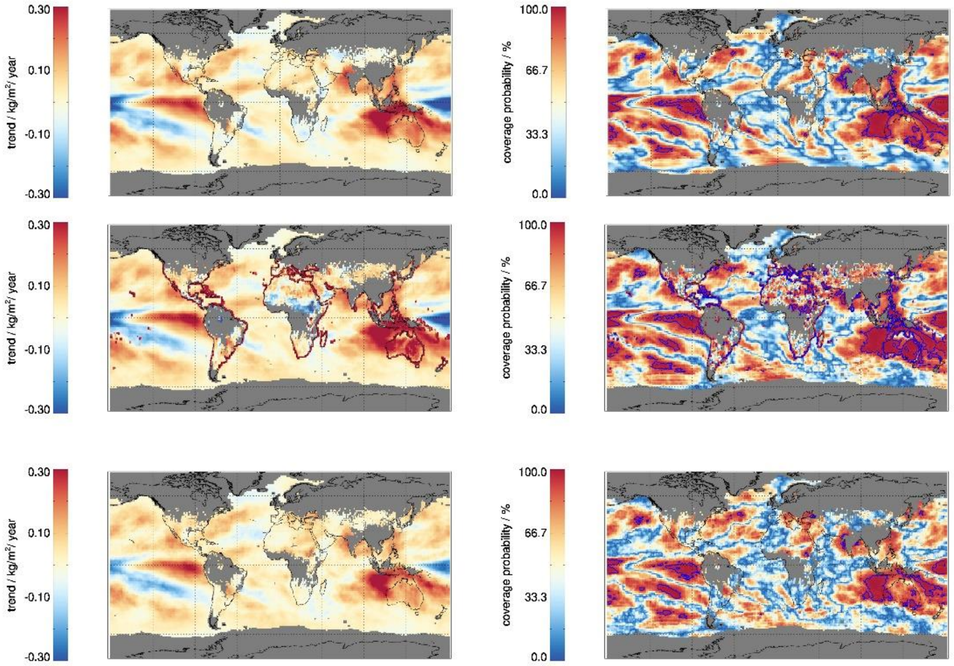

Figure 3-4: The left column shows the spatial distribution of trend estimates in TCWV for (top) ERA5, (middle) CDR-2 and (bottom) AIRS+AMSU. The right column shows the coverage probability with values above the 95% confidence level marked in blue. The map indirectly also shows the global common mask applied to all datasets (grey areas).

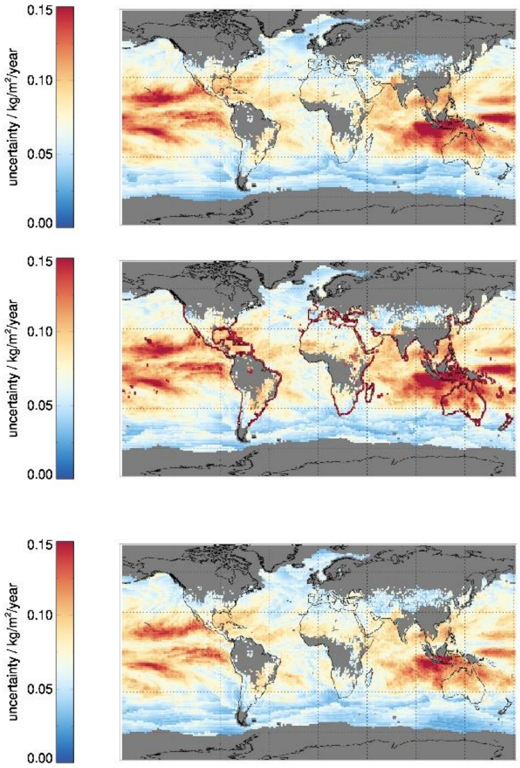

Figure 3-5: Spatial distribution of trend uncertainty estimates in TCWV for (top) ERA5, (middle) CDR-2 and (bottom) AIRS+AMSU v6. Associated trends are shown in Figure 3-4.

3.3.3 Compliance with theoretical expectation

Changes in TCWV are strongly related to changes in surface temperature. This change is expected to follow Clausius–Clapeyron scaling of approximately. 6–7.5 %/K (e.g. Wentz and Schabel, 2000; O'Gorman and Muller, 2010). The assessment of compliance with theoretical expectation largely follows approaches applied within G-VAP (Schröder et al., 2016, 2019). Preparations of CDR-1 and CDR-2 and intercomparison and reference data records were already described in Sections 3.1 and 3.2.

Table 3-1 summarises the results from regression analysis. It includes the regression and correlation for CDR-1, CDR-2, ERA5 and AIRS+AMSU with SST data from ESA CCI and the regression and correlation for CDR-1 with LST data from ESA CCI. Over ocean the values range from 8.22 %/K (ERA5) to 11.92 %/K (CDR-2). In all ocean cases the values are larger than the theoretically expected values. Nonetheless, the associated correlation is fairly large with values around 0.8. In contrast, the regression over land is only 0.53 %/K and thus smaller than the expectation. The uncertainty assigned to the regression values is purely based on the quality of the regression and does not account for uncertainties in TCWV, SST and LST data. We refer to the PVIR v2.1 and to the Group for High Resolution SST (GHRSST, see http://www.ghrsst.org) and PVIRs from ESA SST_cci and ESA LST_cci (see https://climate.esa.int/en/projects/sea-surface-temperature/ and https://climate.esa.int/en/projects/land-surface-temperature/).

The observed values over ocean are different from values published by, e.g. Wentz and Schabel (2000), Mears et al. (2007) and Schröder et al. (2016, 2019). Again, the differences in considered time periods impact results. Impacts can also be expected from differences in utilised methods and time scales (see, e.g. Wentz and Schabel, 2000; Mears et al., 2007; Dessler and Davies, 2010). This is also an indication that the considered temporal coverage and the covered ENSO variability can have an impact on results. The imprint of ENSO on TCWV is not identical between ENSO events (see, e.g. missing lag for the El Niño event in 1987/1988 between SST and air temperature, Wentz and Schabel, 2000). The observed time lag between SST and TCWV and its dependence on ocean basin further impacts the results (Shi et al., 2018). However, results shown in Wentz and Schabel (2000) indicate that this lag can also be a function of event and with that time. Even more so, the local response to ENSO will likely also exhibit variability, as observed by Stephens et al. (2018) for precipitation. The presence of time lags between SST and TCWV during El Niño events, at least occasionally, and the number of observed events impacts the correlation, regression and associated uncertainty and consequently, a comparison to results from the literature is hardly possible when considered periods are different. We further note that different TCWV and SST data records were used in the cited references.

Table 3-1: Results from regression analysis for TCWV from CDR-1, CDR-2, AIRS+AMSU-B and ERA5

Data record	**Global ice-free ocean**		**Global land surfaces**	
	regression ± uncertainty / %/K	**correlation (R^2)**	**regression ± uncertainty / %/K**	**correlation (R^2)**
CDR-2/CDR-1	11.92±0.51	0.78	0.53±0.44	0.01
ERA5	8.22±0.32	0.82	-	-

Data record	**Global ice-free ocean**		**Global land surfaces**	
	regression ± uncertainty / %/K	**correlation (R^2)**	**regression ± uncertainty / %/K**	**correlation (R^2)**
AIRS+AMSU	9.79±0.45	0.76	-	-

In order to discuss potential reasons for the regression being larger (ocean) / smaller (land) than the expectation, a brief discussion of dependencies and assumptions and limitations behind the regression is given. This is largely based on Mieruch et al. (2014) and was slightly adapted and extended: Following Hyland and Wexler (1983) saturation vapour pressure is a function of air temperature and change in air temperature. Saturation vapour pressure can be transferred into a change in mixing ratio assuming constant relative humidity and pressure. For a temperature change of 1 K the expected change in mixing ratio is between 6% at 300 K and 7.5% at 275 K. The relationship between TCWV and surface temperature is affected by advection, precipitation, and other small-scale and regional events, which impact equilibrium between surface and atmosphere. Also, surface temperature and TCWV instead of near-surface air temperature and mixing ratio are considered here. This might lead to an amplification of the regression over ocean (Trenberth et al., 2005). Over land, the relation between air temperature and surface temperature is complex and locally the difference between air and surface temperature reaches a few Kelvin. This depends on various factors, such as local time, cloudiness and surface type (e.g. Good, 2016 and Rayner et al., 2020). It is thus difficult to estimate its impact on regression. In contrast to ocean, the potential flux of water vapour into the atmosphere can be limited over land and is fairly complex (Byrne and O’Gorman, 2016). Such an input flux depends on various processes and parameters, among others, advection from ocean to land, presence of surface water (lakes, rivers, swamps, etc.), soil moisture, and vegetation density, type and physical stress. It is noted that temperature increases more rapidly over land than over ocean (e.g. Byrne and O’Gorman, 2013) and this itself will also impact differences in regression over land and ocean. Nonetheless, Byrne and O’Gorman (2016) conclude that the moisture transport from the ocean is the dominating process for changes in specific humidity over land while evapotranspiration processes play an important role for changes in relative humidity over land. Finally, the presence of increased SST and TCWV over ocean during El Niño events might lead to larger transport of moisture from ocean to land. At the same time increased LST might not be present and can thus further contribute to a reduced correlation between LST and TCWV.

3.4 Conclusions

In this section the following analysis was carried out using TCWV from the CDR-1, CDR-2, ERA5 and AIRS+AMSU data records:

- Contribution of the annual cycle and ENSO to variability
- Trend estimation on grid-basis and for large scale regional averages
- Compliance analysis with theoretical expectation following Clausius–Clapeyron using regression.

Based on the presented results it can be concluded that the spatial representation of variability, trends and associated uncertainties are very similar between the considered data records. However, trend estimates and regression values using near global data differ between AIRS+AMSU, ERA5 and CDR-1, CDR-2, with CDR-1 and CDR-2 exhibiting the largest values. A regression analysis over land is pursued for CDR-1 only because the changes in TCWV over land are driven by advection from oceans and not by LST or surface air temperature.

A comparison to published trend estimates and regression results is hardly possible, mainly given the differences in temporal coverage and ENSO coverage but also due to differences in spatial coverage, utilised data records and applied methods.

Given the fairly short temporal coverage and the presence of an El Niño event at the end of the considered time series, the presented trend estimates cannot be considered as long-term climate trends.

4. ANALYSIS OF TIME SERIES, TRENDS AND VARIABILITY OF VERTICALLY RESOLVED WV PRODUCTS (CDR-3)

Daan Hubert (BIRA-IASB), Jean-Christopher Lambert (BIRA-IASB)

The vertically resolved water vapour data products developed by ESA's WV_cci project are compared to similar Climate Data Records produced by NASA (GOZCARDS, https://gozcards.jpl.nasa.gov) and NOAA (SWOOSH, http://www.esrl.noaa.gov/csd/swoosh). The objective is to assess the value of the CCI data products for climate studies, through a comparative analysis of known spatial and temporal patterns, variability and trends. Past studies concluded to different long-term trends in water vapour, depending on the analysis methods and data records being used (e.g. Hegglin et al., 2014 and Hurst et al., 2011). Here, we reassess the (dis)agreement between current satellite-based monthly-zonal-mean CDRs by comparing the parameter estimates for different (geophysical) patterns inferred by Multiple Linear Regression analyses.

4.1 Monthly zonal mean H_2O Climate Data Records

This assessment includes four CDRs: CCI CDR-3 v0 (ATBD, 2020), SWOOSH v2.6 (Davis et al., 2016), GOZCARDS v1.01/1.02 (Froidevaux et al., 2015) and GOZCARDS v1.10. They all report monthly mean H_2O VMR on a fixed pressure and latitude grid. These CDRs are constructed using different sets of satellite sensors, different Level-2 data versions and different merging algorithms. Each of these choices can have an important impact on the short-term and long-term temporal stability of the CDR. The four H_2O CDRs are not independent as they all include HALOE H_2O retrievals in the 1991–2005 period and Aura MLS data since 2005. The number of sensors included is largest for the CCI data record (11), hereby distinguishing itself clearly from SWOOSH (6) and GOZCARDS (3–4).

Recent trends (since 2005) are fairly sensitive to the Aura MLS data version used. The latest Aura MLS data processor (v5) includes corrections which reduce the positive drift in H_2O retrievals noticed in earlier data versions v3/v4 (Hurst et al., 2016; Livesey et al., 2021). Hence, it is expected that CCI CDR-3 v0 and GOZCARDS v1.10 exhibit smaller positive recent trends (both using Aura MLS v5) than GOZCARDS v1.01/1.02 and SWOOSH v2.6 (both using Aura MLS v3/v4). The latest GOZCARDS incarnation uses the same merging algorithm as its predecessor, but does not include UARS MLS data which may lead to differences in the early 1990s.

4.2 Baseline regression model

Let $\{Y_t\}$ denote the set of monthly H_2O VMR measurements, for a given pressure level and latitude band. Changes in stratospheric water vapour have been attributed to or are co-variant with a number of processes (e.g., Hurst et al., 2011, Dessler et al., 2014; Hegglin et al., 2014; Lossow et al., 2017a, 2017b, 2018; Schieferdecker et al., 2015; Diallo et al., 2018; Randel et al., 2019). Here, we assume a linear response of H_2O VMR to each of the following processes

$$Y_t = \mu + A_t + QBO_t + X_t + N_t.$$

In this model, μ represents the mean H2O VMR over the Jan 2005 – Dec 2015 period. Seasonal changes are modelled as a sum of two Fourier components (12 and 6 month period, AO and SAO): $A_t = \sum_{j=1}^{2} \alpha_{j,1} \cos(2\pi jt/12) + \alpha_{j,2} \sin(2\pi jt/12)$. The Quasi-Biennial Oscillation (QBO) is parameterised using two (orthogonal) principal components of Singapore winds at 30 hPa and 50 hPa[1]: $QBO_t = \beta_1 QBO_{PC1,t} + \beta_2 QBO_{PC2,t}$. Long-term changes are parameterised as a continuous series of three linear trends X_t inflecting in January 1998 and in January 2004. Left-over noise N_t is modelled as a first-order autoregressive process : $N_t = \phi N_{t-1} + \epsilon_t$.

The set of parameter coefficients θ is inferred using a generalised least-squares regression technique that accounts for data gaps. This regression is applied to all pressure levels and latitude bands independently, on the native grid of the CDR. Reported H_2O VMR errors are not considered by the regression since the contribution of actual measurement uncertainty and geophysical variability varies between CDRs. The MLR implementation utilised here can be downloaded from https://arg.usask.ca/docs/LOTUS_regression/index.html

Figure 4-1 illustrates the parameters estimated for the CCI CDR-3 data record.

---

[1] *From http://www.geo.fu-berlin.de/met/ag/strat/produkte/qbo/qbo.dat*

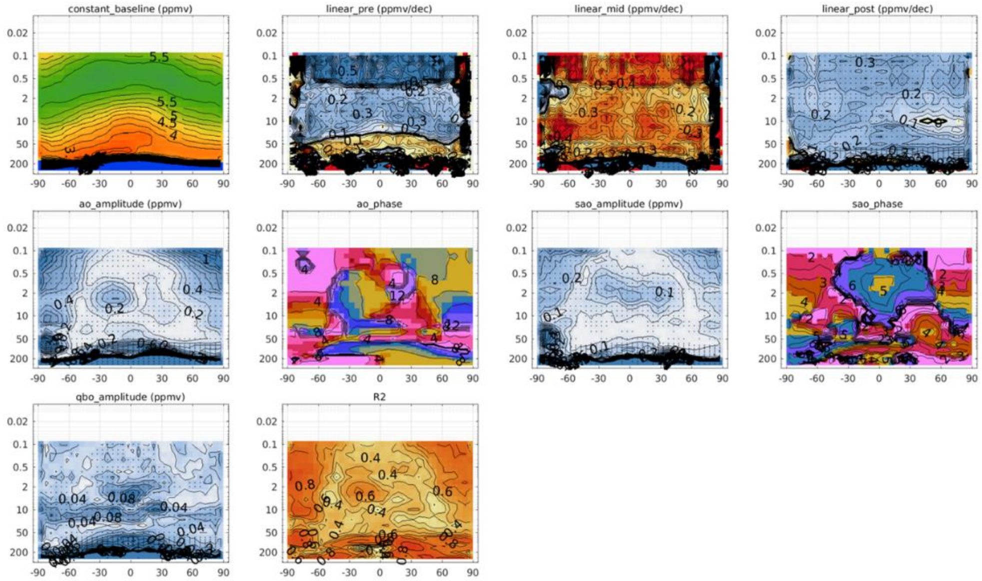

Figure 4-1: Pressure–latitude cross-section of regression parameters estimated from CCI CDR-3: the 2005–2015 mean (top left), three linear trend terms (top row; pre: 1984–1997, mid: 1998–2003, post: 2004–2018), followed by amplitude and phase of the annual (ao), semi-annual (sao) and quasi-biennial (qbo) oscillations. The last panel shows the coefficient of determination R^2. Stippled cells show statistically significant parameters (2σ). The unit is displayed at the top of each panel.

4.3 Comparison of parameter estimates

Parameter coefficient estimates $\hat{\theta}$ are expressed as *ppmv* or as *ppmv/decade*. Relative parameter coefficient estimates $\hat{\theta}_r$ (in *%* or *%/decade*) are obtained by dividing by the estimate of the multi-annual mean: $\hat{\theta}_r = 100 \times \hat{\theta}/\hat{\mu}$. Difference statistics use the CCI CDR-3 as a reference: $\hat{\delta} = \hat{\theta} - \hat{\theta}_{CCI}$ (ppmv or ppmv/decade) and $\hat{\delta}_r = \hat{\theta}_r - \hat{\theta}_{r,CCI}$ (% or %/decade)[2]. The uncertainty of the differences is obtained by assuming uncorrelated, Gaussian coefficient errors: $\hat{\sigma}_\delta = \sqrt{\hat{\sigma}_\theta^2 + \hat{\sigma}_{\theta CCI}^2}$. Parameter (difference) estimates are considered statistically significant when their significance exceeds the 5% level : $|\hat{\theta}| > 2\hat{\sigma}_\theta$ or $|\hat{\delta}| > 2\hat{\sigma}_\delta$.

4.4 Multi-annual mean (Jan. 2005 – Dec. 2015)

Figure 4-2 (top row) displays the multi-annual mean distribution of H_2O for each of the four CDRs. The general spatial structure is in agreement between all CDRs: very high

---

[2] *To avoid any confusion, quoted percentage differences of the relative parameters are not defined as* $100 \times \frac{\theta}{\theta_{CCI}}$.

H_2O VMRs below the tropopause, a dry lower stratosphere, especially in the tropics, and gradually increasing VMRs at higher altitudes and latitudes. Differences in the multi-annual mean (Figure 4-2, bottom) between the CDRs exhibit a weak spatial structure.

CCI CDR-3 is drier than the other CDRs across almost the entire stratosphere and mesosphere. In the stratosphere, the negative bias of CCI is about 0.5–0.8 ppmv or 10–14% (GOZCARDS v1.10), 0.6–1.0 ppmv or 14–18% (GOZCARDS v1.01/1.02) and 0.7–1.5 ppmv or 20–25% (SWOOSH v2.6). In the mesosphere, the negative bias of CCI amounts to 0.7–1.2 ppmv or 13–24% (GOZCARDS v1.10) and 1.0–1.5 ppmv or 16–28% (GOZCARDS v1.01/1.02). In other parts of the atmosphere, the CCI CDR-3 multi-annual mean is wetter than other CDRs. Below the 150–170 hPa level CCI data exhibit a clear positive bias w.r.t. SWOOSH of 20–45% in the tropics and 20–70% in the polar regions. In the Antarctic lower stratosphere (~100 hPa) the CCI multi-annual mean is 4% (SWOOSH) to 10–12% (w.r.t. GOZCARDS) larger.

Multi-annual mean H2O of CCI differs clearly from GOZCARDS and SWOOSH, while the latter are in better mutual agreement. The use of (many) more sensors and the different merging approach (e.g. the transfer standard) may lead to this difference.

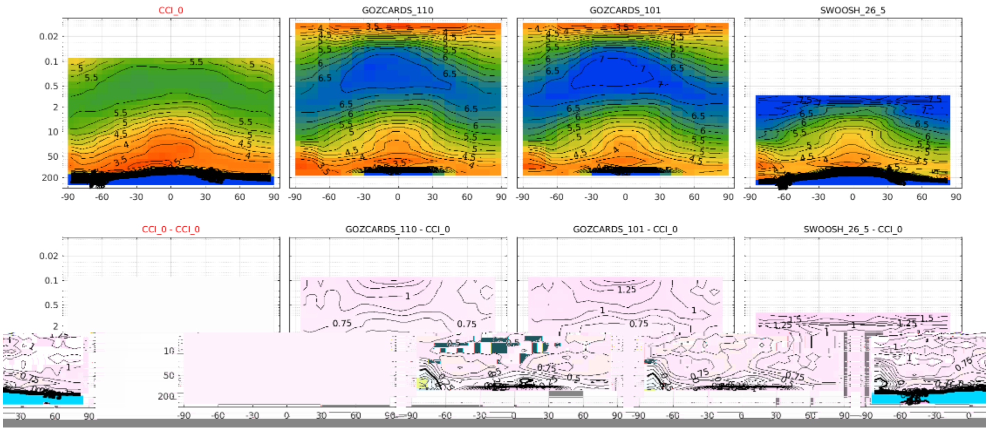

Figure 4-2: Top: pressure–latitude cross-section of the mean H_2O VMR between January 2005 and December 2015 for four CDRs (left to right: CCI CDR-3 v0, GOZCARDS v1.10, GOZCARDS v1.01/1.02 and SWOOSH v2.6). Bottom: absolute difference of each CDR w.r.t. CCI CDR-3 (positive values indicate that CCI is drier). All units are ppmv.

4.5 Annual cycle

The strongest periodic variation in the CDRs is a 12-month (annual) oscillation (AO). This cycle is clearly detected across the entire stratosphere and mesosphere (Figure 4-3). Its amplitude (i.e., half of the peak-to-peak range) is especially large in the lower stratosphere (>0.6-0.8 ppmv, >8-20%), in the upper stratopause around 20°S (0.4-0.5 ppmv, 8-10%) and in the polar regions (>0.6 ppmv, >8%). Lossow et al. (2017a, 2017b) discuss in detail the processes underlying the annual cycle, leading to the observed spatial structure in amplitude (Figure 4-3) and phase (Figure 4-4).

The agreement between CDRs of the magnitude and spatial structure of annual cycle properties is overall fairly good. CCI CDR-3 amplitudes are smaller than other CDRs in the tropical lower stratosphere (by 0.1 ppmv, 2%) and the polar middle stratosphere and mesosphere (by >0.2 ppmv, 2%). GOZCARDS exhibits a weaker cycle (not more than 0.05 ppmv) than CCI, in large parts of the upper stratosphere. Across the entire upper stratosphere percentage amplitudes CCI are (~0.5–1%) larger than all other CDRs. Sign changes between the difference in absolute and relative parameter estimates are a result of differences in the multi-annual mean H_2O VMR for CCI and other CDRs (discussed in Section 4.4).

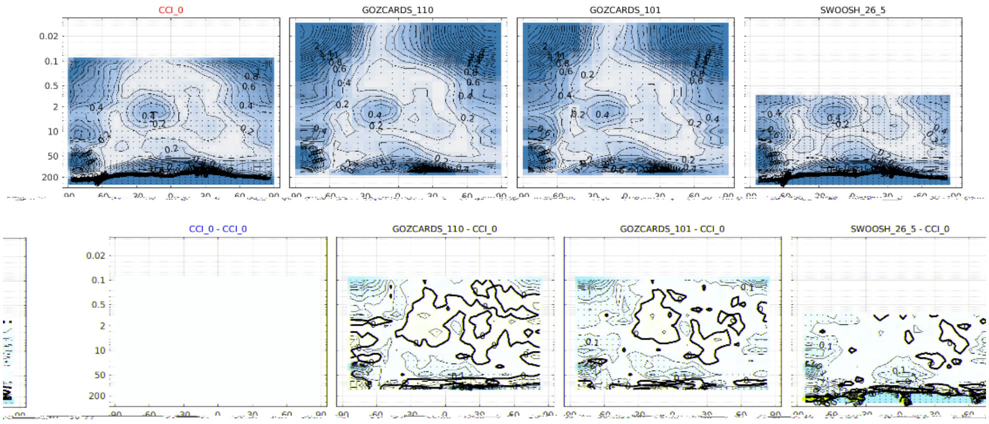

Figure 4-3: Top: pressure–latitude cross-section of the amplitude of the annual cycle for four CDRs. Bottom: absolute difference CDR minus CCI CDR-3 (pink: positive, cyan: negative). The zero level is indicated as a thick black contour. All units are ppmv. Stippled cells indicate statistically significant estimates (2σ).

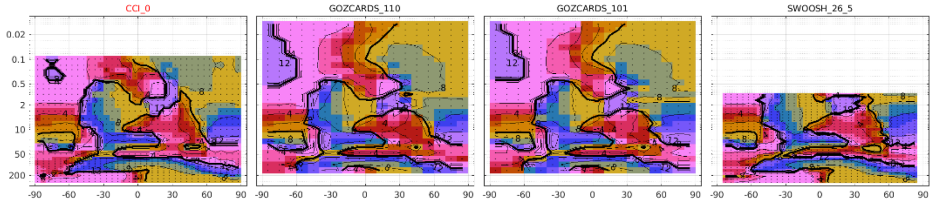

Figure 4-4: As Figure 4-3, but for the phase of the annual cycle. The thick contour line indicates July. Unit is month number.

4.6 Semi-annual cycle

Clear signs of a six-month oscillation (SAO) are detected across the entire atmosphere, except in the middle stratosphere at low and middle latitudes. The amplitudes are largest (0.2 ppmv, 4%) in the lowermost stratosphere, the tropical upper stratosphere (0.2 ppmv, 3–4%) and across the polar stratosphere and mesosphere. Spatial structure of amplitude (Figure 4-5) and phase (Figure 4-6) agree with earlier reports (e.g. Lossow et al., 2017a).

Differences between the CDRs are small and exhibit little spatial structure, except for a region with larger differences in the Antarctic. Amplitudes agree mostly within 0.02 ppmv or 0.5%. Patterns in SAO phase are very similar between CDRs.

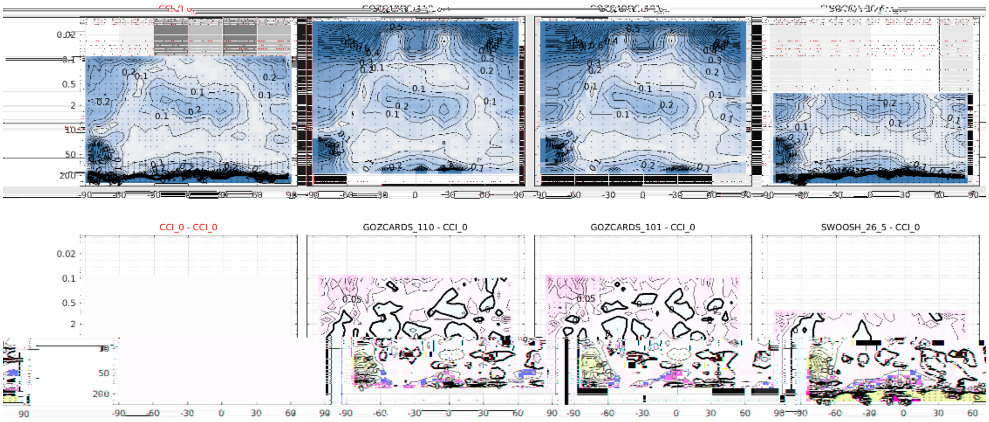

Figure 4-5: As Figure 4-3, but for the amplitude of the semi-annual cycle. All units are ppmv.

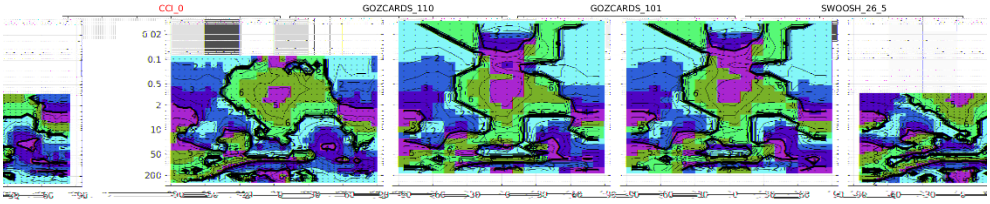

Figure 4-6: As Figure 4-4, but for the phase of the semi-annual cycle. The thick contour indicates April. Unit is month number.

4.7 Quasi-Biennial Oscillation

The response of H_2O to QBO is particularly strong around 3–5 hPa in the tropics (0.08–0.12 ppmv, 1.5–2.5%), between 10 and 20 hPa (0.06–0.10 ppmv, 1.5–2.5%) in the tropics and mid-latitudes, and across the entire upper troposphere (>0.10 ppmv, >3%).

As for the other periodic cycles, the spatial structure of QBO properties is very similar for the different CDRs. Regions where the QBO is statistically significant coincide for all data records. Generally the difference in amplitude is less than 0.01 ppmv or ~0.2% and exhibits no clear systematic structure in the sign of the bias.

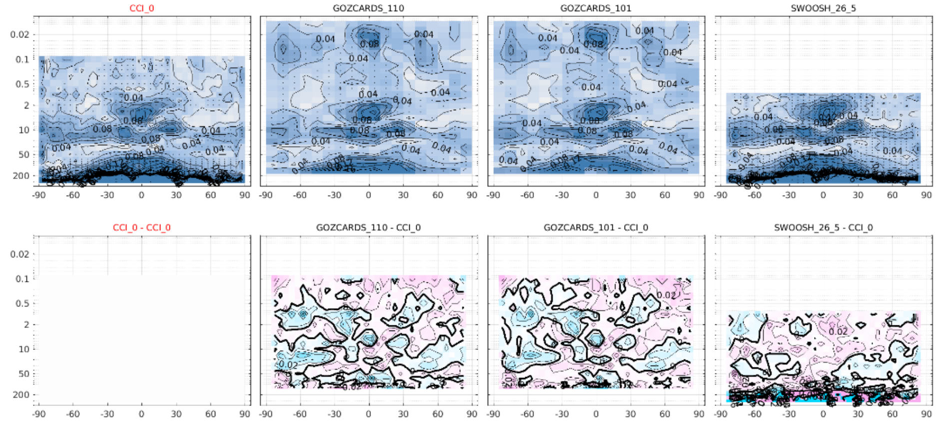

Figure 4-7: As Figure 4-3, but for the amplitude of the QBO. All units are ppmv.

4.8 Trends

Figure 4-8 displays the long-term evolution in CCI CDR-3 H_2O data for several latitude bands and pressure levels. The residuals are obtained by subtracting the regressed AO, SAO and QBO cycles from the observations, then smoothing using a 10-year moving mean window (black). Also shown is the regressed trend model (red) consisting of three piecewise continuous linear trends inflecting at January 1998 and January 2004. Such a model is a reasonable description in large parts of the atmosphere. However, in some regions and for some periods there are signs of overfitting. This is mostly the case for the trend estimates prior to 2004 in the mesosphere and at high latitudes. These estimates should therefore be interpreted with care. Trends since 2004, on the other hand, are well modelled across the entire probed atmosphere.

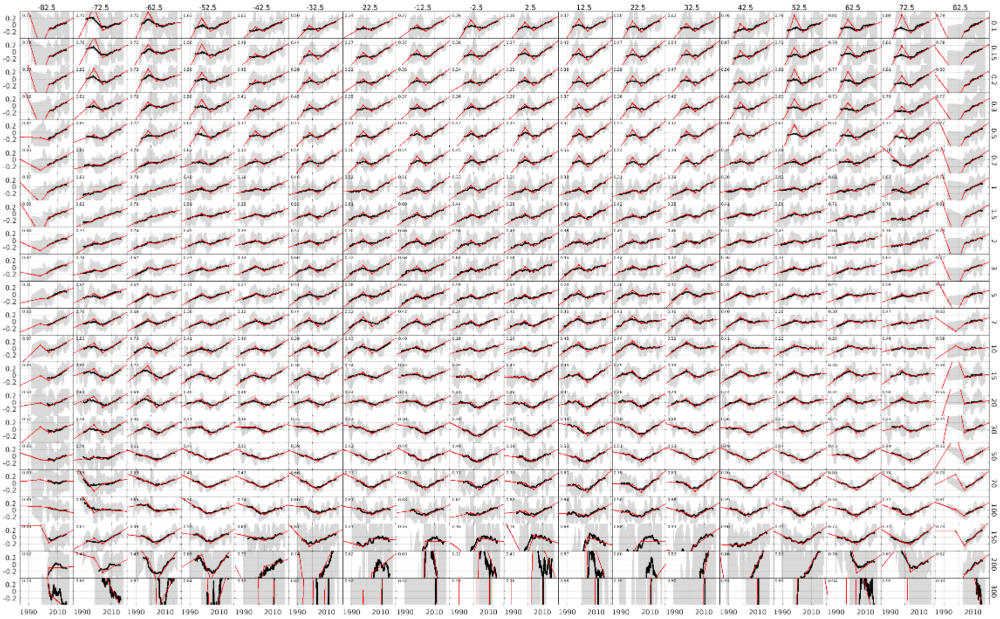

Figure 4-8: Time series of CCI CDR-3 residuals after subtraction of the regressed AO, SAO and QBO cycles, then smoothed over 10 years to highlight long-term changes (black). Grey shades indicate shorter-term changes: 2-year smoothed residuals and their standard deviation. The trend component of the MLR fit is shown in red. Each panel represent a latitude bin (columns) and pressure level (rows). Units are ppmv.

The spatial structure of each of the three trends for all CDRs, and their difference w.r.t. CCI, is shown in Figure 4-9 to Figure 4-11. The long-term behaviour differs considerably between the CDRs.

4.8.1 Prior to 1998

GOZCARDS trends prior to 1998 are not comparable to CCI or SWOOSH results due to a much later start of the CDR (1991 versus mid 1980s). These are therefore not further discussed here. Also not discussed are the CCI trend results above the 0.7 hPa level since affected by a considerable positive bias due to overfitting.

Figure 4-9 (top) shows that, during this early period, both CCI and SWOOSH exhibit highly significant (>3–4σ) positive trends in the middle and upper stratosphere (up to 0.35 ppmv/decade or 8%/decade) and significant negative trends in the lower stratosphere (up to -0.2 ppmv/decade or -6%/decade). Trends in the tropical upper troposphere vary in sign in magnitude but are not significant.

While CCI and SWOOSH trends are statistically significant, the difference in trend between these CDRs is not. Percentage trends (%/decade) for CCI are mostly more positive (or less negative) than for SWOOSH (Figure 4-9, bottom). However, absolute trends (ppmv/decade) for CCI are more negative (or less positive) than for SWOOSH (not shown). The sign change between percentage and absolute trends is a result of the difference in multi-annual mean between these CDRs. But, again, CCI and SWOOSH trends are consistent when errors are considered.

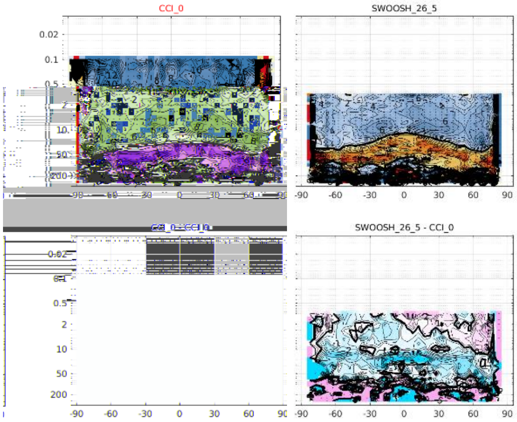

Figure 4-9: As Figure 4-3, but for the trend between start of CDR and December 1997 (%/decade). GOZCARDS trends prior to 1998 are not shown since they are incomparable to CCI or SWOOSH results (see text).

4.8.2 Between 1998 and 2003

A highly coherent picture of significantly decreasing H_2O VMRs is seen during this period across the lower and middle stratosphere for all CDRs, including the smaller scale spatial structure. However, trend magnitudes do differ between CDRs in large parts of the stratosphere.

GOZCARDS trends are generally more than 5%/decade more negative than the other CDRs. At this point, it is unclear how reliable the GOZCARDS estimates are. Additional work will be needed to verify whether this bias is related to overfitting by the MLR (due to the shorter data record?) or results from actual different temporal behaviour in the GOZCARDS time series.

SWOOSH trends are 4-5%/decade larger (and positive) than CCI or GOZCARDS (which are negative) across the upper stratosphere (above the 5 hPa level). The difference is statistically significant in this region. At lower altitudes, SWOOSH trends remain larger (i.e. less negative) than other CDRs but the difference is less pronounced. At 20 hPa, the SWOOSH trend is about -8%/decade compared to −10%/decade for CCI and -15%/decade for GOZCARDS.

A discontinuity appears in the vertical domain for CCI trends around 0.7 hPa. This is likely a result of the overfitting issue reported earlier. Hence, additional work will be needed to consolidate CCI trend estimates in the mesosphere. At this point the negative mesospheric trends maybe be overestimated.

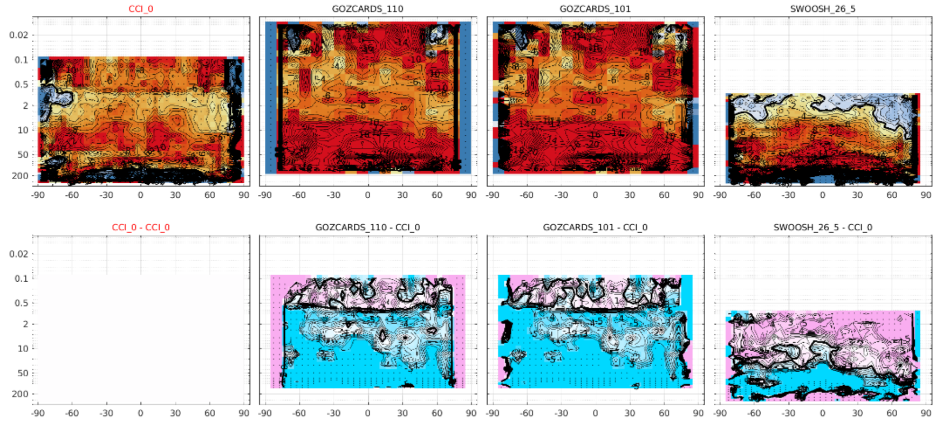

Figure 4-10: As Figure 4-3, but for the trend between January 1998 and December 2003 (%/decade).

4.8.3 Since 2004

Since early 2004, all CDRs exhibit very significant (>3–4σ) increases in H_2O across most of the atmosphere. Some regions with insignificant, negative trends lie in the tropical UTLS (-2%/decade), the polar UTLS (-4%/decade) and between 5 and 20 hPa at Northern mid- and high-latitudes (1–2%/decade). Elsewhere, positive trends are found of up to 8–10%/decade in the lowermost stratosphere, and 4–6%/decade in the middle and upper stratosphere and mesosphere.

Directly comparing both GOZCARDS versions, we find that v1.10 trends are 2–3%/decade smaller (less positive) than v1.01/1.02 trends across the entire atmosphere. This difference is in line with expectations from the drift correction applied to the recent Aura MLS H_2O data version (Livesey et al., 2021). Hence, these findings can be explained by the different Aura MLS data version.

Differences between SWOOSH v2.6 and GOZCARDS v1.01/1.02 are small (<1%/decade) and insignificant, both largely rely on Aura MLS for data from recent decades.

While CCI trends are mostly larger (often >1%/decade) than those inferred from GOZCARDS or SWOOSH, these differences are statistically insignificant in large parts of the atmosphere. One notable exception is that CCI trends are 3–4%/decade more positive than GOZCARDS v1.10 below the 10 hPa level, a difference that is significant. Differences of 2–3%/decade between these records are significant in the tropical upper stratosphere as well. Hence, it seems that the inclusion by CCI of additional sensors and not just Aura MLS in the past 15 years leads to significantly different long-term trends in CCI when compared to GOZCARDS or SWOOSH.

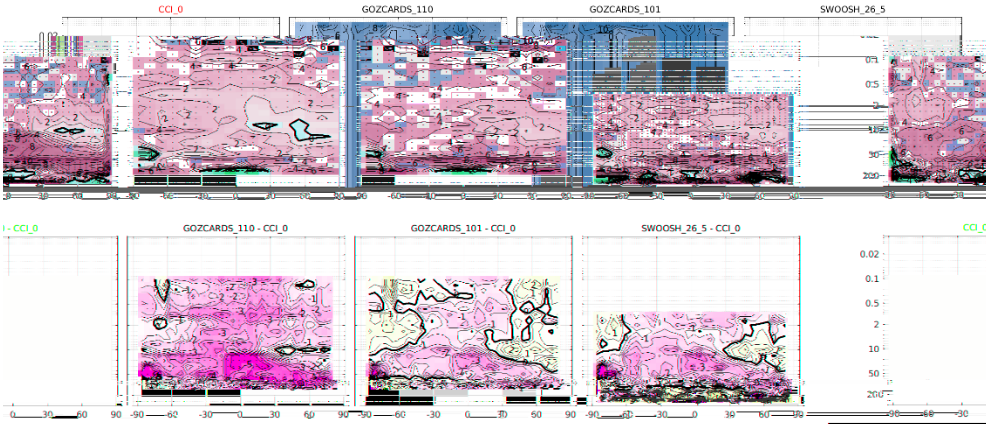

Figure 4-11: As Figure 4-3, but for the trend between January 2004 and end of CDR (%/decade).

4.9 Conclusions

The CCI CDR-3 data record is constructed from a different, considerably larger set of limb sensors than GOZCARDS and SWOOSH, while the latter are based on a similar set of input data. The challenge of the CCI approach is then to obtain accurate offsets for more sensors but with the potential benefit of obtaining a data record less sensitive to errors in one of the input data sets (e.g. sampling bias, drift).

CCI CDR-3 complements the GOZCARDS and SWOOSH data records in terms of spatio-temporal coverage and sampling. Compared to GOZCARDS, the CCI time series start up to seven years earlier (depending on latitude/pressure), has a higher vertical and latitudinal sampling resolution, extends into the troposphere but does not cover the upper mesosphere. Compared to SWOOSH, the CCI record starts up to two years earlier and covers the mesosphere, but offers less spatio-temporal sampling resolution.

Differences in the multi-annual mean (Jan. 2005 to Dec. 2015) inferred from the CDRs are generally statistically significant. The CCI multi-annual mean is clearly smaller than the other CDRs in the stratosphere and mesosphere, by 0.5–1.5 ppmv (or ~10–25%). In contrast, at altitudes below the 150 hPa level (by up to 20–70%) and in the Antarctic lower stratosphere (by 4–12%), the CCI multi-annual mean is biased high relative to the other CDRs.

The dominant patterns of geophysical cycles in CCI CDR-3 are well represented across different temporal and spatial scales. Amplitude and phase of (quasi-)periodic cycles (annual, semi-annual, QBO) generally agree very well with those obtained for GOZCARDS or SWOOSH.

A fairly coherent picture of the longer-term evolution in H_2O emerges from the CDRs. Trends prior to 1998 are mostly positive (and negative in the lower stratosphere), between 1998 and 2003 they are mostly negative and since 2004 again mostly positive. While the inferred trend values differ, often by several %/decade, these differences are generally statistically insignificant. GOZCARDS trends prior to 1998 are incomparable to the other CDRs due to the much later start of the record. Poor agreement is found over the (fairly short) 1998–2003 period during which significant differences are noted in the upper stratosphere (SWOOSH biased high by 4–5%/decade) and below the UTLS. Significant differences in trends since 2004 are noted between CCI and GOZCARDS v1.10, the latter being 2–4%/decade smaller. Both records include Aura MLS v5 data for this time period. Hence, the additional sensors in the CCI record seem to lead to a larger change in the long-term behaviour than the presence of a residual drift in Aura MLS v4 data (used by SWOOSH and GOZCARDS v1.01/1.02).

5. ATMOSPHERIC MOISTURE TRANSPORT

Jorge Eiras-Barca (U. Vigo), Luis Gimeno (U. Vigo)

In this section it is analysed how well do ERA5 and ERAIn solve integrated water vapour (IWV) in regions of particular interest for atmospheric moisture transport processes, particularly atmospheric rivers (ARs; e.g. Gimeno et al., 2014) and nocturnal low-level jets (LLJs; e.g. Algarra et al., 2019a). ERA5 and ERAIn are the most frequently used reanalyses in Lagrangian particle dispersion models and also in moisture tracer simulation both within Eulerian and Lagrangian perspectives (e.g. Eiras-Barca et al., 2017; Algarra et al., 2019b). The cited tools are mostly used to analyse the large moisture transport phenomena, as well as the source and sink regions of the atmosphere–ocean and atmosphere–lithosphere interactions.

CDR-2 is used here as a set of reliable and comprehensive observations that are used to test the goodness of both ERAIn and ERA5 in strategic source regions for the two most important moisture transport processes: ARs and LLJs.

Particularly, the resemblance between the reanalysis and the CDR-2 datasets is tested in strategic regions for moisture transport processes in three different ways:

1. Plots of mean monthly BIAS (ERA5 vs CDR-2 and ERAIn vs CDR-2) using CDR-2 monthly data with a resolution of 0.5º × 0.5º.

2. Plots of mean daily temporal correlation (ERA5 vs CDR-2 and ERAIn vs CDR-2) using CDR-2 daily data with a resolution of 0.5º × 0.5º. The results are presented annually, which also allows a comparison between the different years of the period under consideration (2003–2017).

3. Considering more than 30×10^3 AR events and more than 8×10^3 LLJs events detected worldwide from 2003 to 2017 (Algarra et al., 2019a, 2020); the probability density functions (pdf) of IWV (ERA5 vs CDR-2 and ERAIn vs CDR-2) are included in the analysis, first having divided the global domain into a set of independent regions of interest.

The full results are available in Eiras-Barca et al. (2022). Here, the mean monthly BIAS (Reanalysis–CDR-2) throughout the period 2003–2017 is shown as example result. Regions of interest for moisture transport processes are highlighted with dotted polygons. Also, the two most important tropical rainforests are highlighted in red (Figure 5-1 and Figure 5-2).Regions of interest for relevant moisture transport processes (particularly atmospheric rivers, black dotted polygons) are located offshore in regions where the reanalysis and the CDR-2 observations show an overall good agreement. These regions are characterised by low biases both in the Northern and Southern Hemispheres. The latter is true both for ERA5 and ERAIn, which show a good agreement.

In general Eiras-Barca et al. (2022) conclude that the regions of high interest for moisture transport phenomena show a high degree of agreement between both reanalyses and CDR-2. The BIAS are, in general, lower than 2 mm —with low standard deviations in their errors— and the temporal correlations —calculated on a daily time scale— are higher than 0.8.

Discrepancies are accentuated with ERAIn compared to ERA5, as well as in period P5; corresponding to the year 2017. Similarly, relatively high discrepancies are observed in the regions corresponding to tropical forests. Although these regions are rich in moisture content, they do not play any role as source regions for ARs and LLJs. Therefore, it can be concluded that the reanalyses that have been used in recent times have been providing and will provide reliable TCWV information to moisture transport models that analyse sources, sinks and moisture transport phenomena.

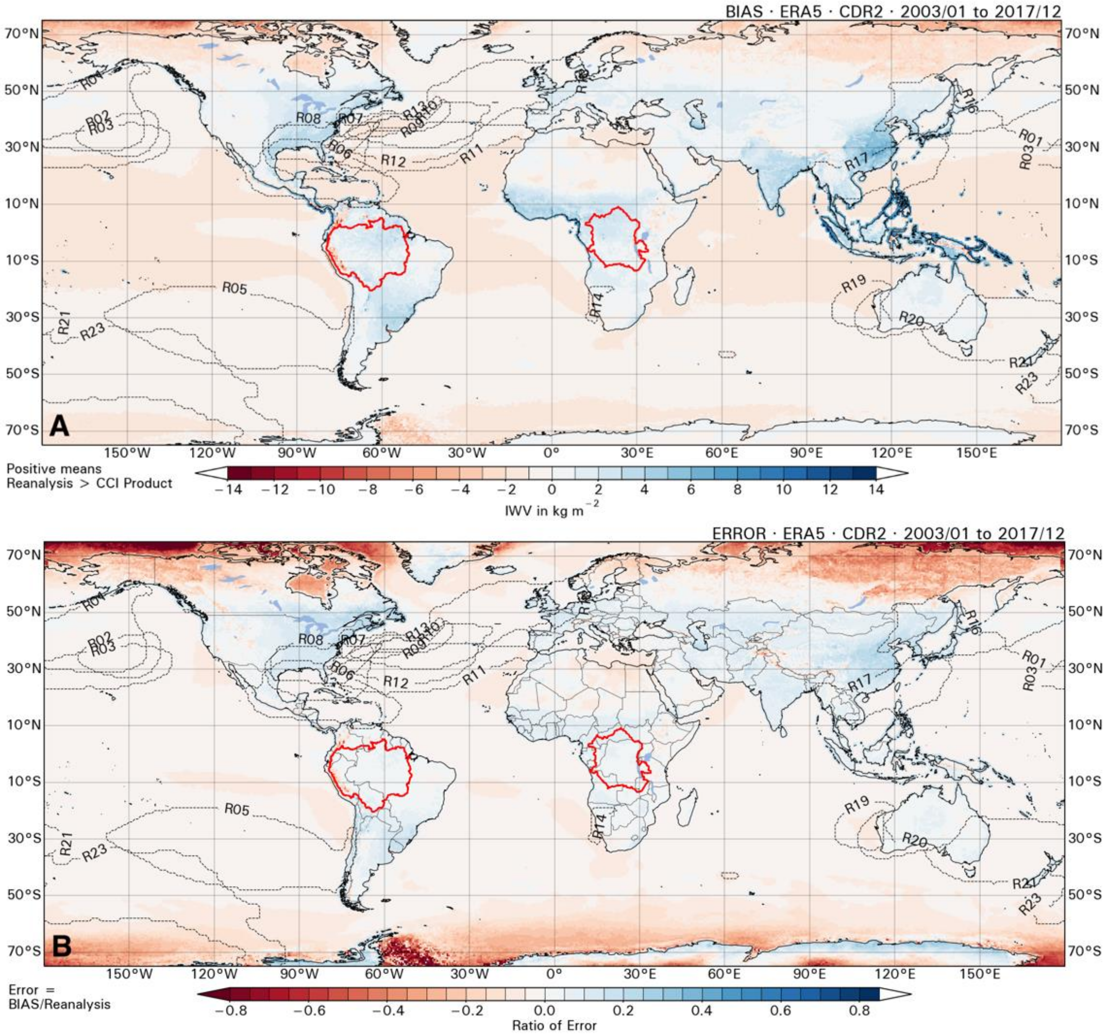

Figure 5-1: (A) The mean monthly BIAS ERA5 – CDR-2 and (B) the ratio of error. Source regions for atmospheric river activity are highlighted with black dotted polygons. The two most relevant tropical rainforests are also highlighted with red polygons.

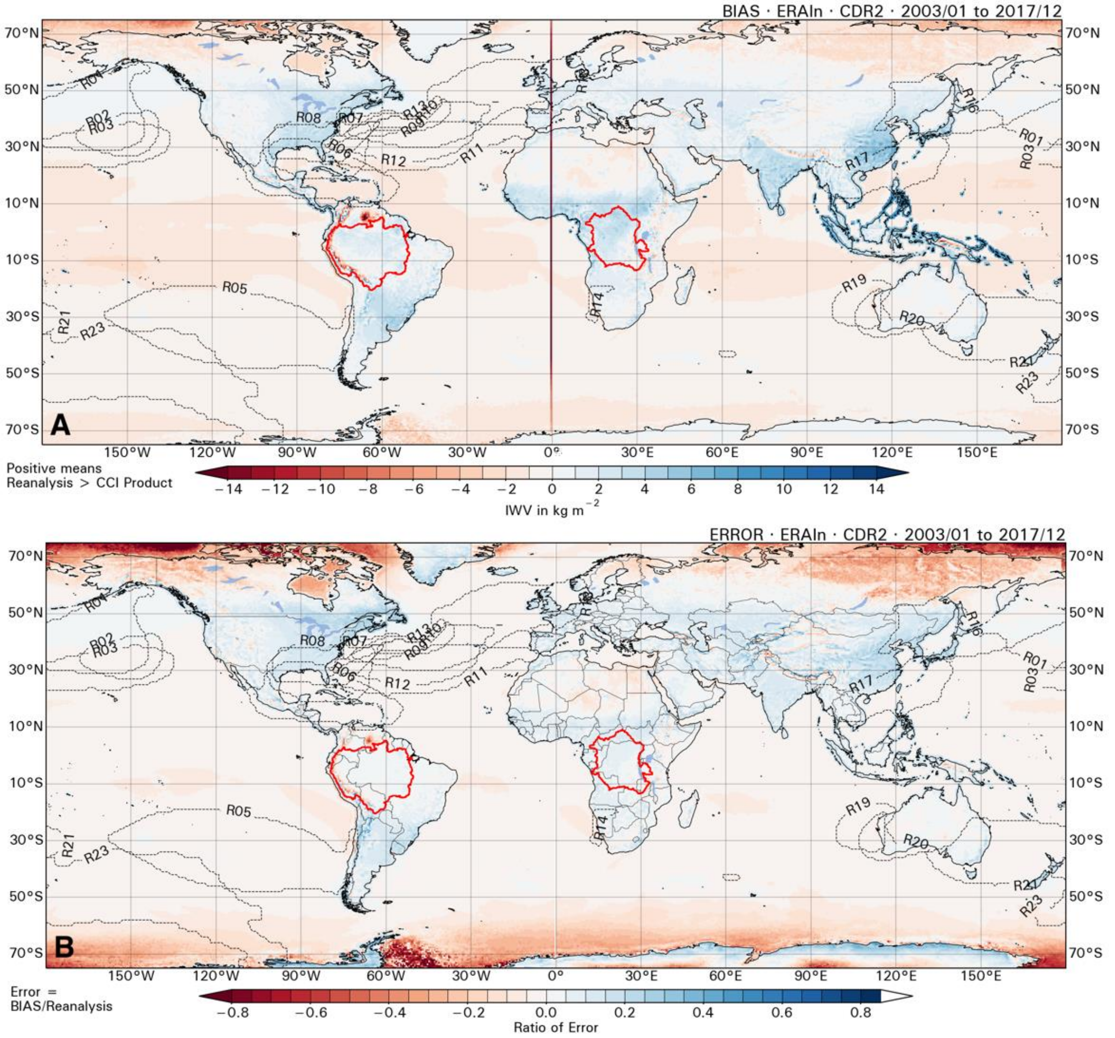

Figure 5-2: (A) The mean monthly BIAS ERA Interim – CDR-2 and (B) the ratio of error. Source regions for atmospheric river activity are highlighted with black dotted polygons. The two most relevant tropical rainforests are also highlighted with red polygons.

6. CLIMATE STUDIES USING CMIP6 AND ERA5

Jia He (UVSQ), Hélène Brogniez (UVSQ)

Today, how the global atmospheric water cycle will adjust as climate warms is still not fully understood, while the radiative importance of the atmospheric water in maintaining the thermal energy balance of the Earth system is undebated. (The connection between temperature, water vapour and infrared radiation creates a positive feedback that further warms the global climate from an external forcing; *cf*. IPCC 2013, 2018 and the WCRP strategic plan for the 2019–2029 decade.) However, the representation of the complexity of cloud-moisture–surface interactions remains a central challenge for climate models, and thus restrains our confidence in future climate modifications at all spatial scales.

The increase in surface temperature from anthropogenic forcing yields an observed increase in the atmospheric water vapour (Soden et al., 2005), in accordance with the laws of thermodynamics. This increase in water vapour available in the atmosphere reinforces convergence in tropical regions, with more rainfall in regions particularly sensitive to hydrological changes, and also reinforces divergence in the subtropics (Held and Soden, 2006). This can be summed up as "wetter regions are wetter and drier regions are drier".

Evaluation of the ability of climate models to represent the distribution and variation of tropospheric water vapour according to known patterns of the Hadley–Walker circulation where large-scale subsidence is associated with a dry troposphere and where large-scale ascent is associated with convection and thus a moister troposphere.

6.1 CMIP6 models

Table 6-1 lists the seven CMIP6 models that have been selected for this study. This selection is based on the availability of specific humidity (hus) with sufficient vertical resolution (≥ 19 levels) to calculate total column water vapour, and the corresponding atmospheric vertical velocity (wap), cloud fraction (cl), precipitation (pr) at daily frequency.

The total column water vapour (TCWV) is calculated from all vertical levels available using:

$$TCWV = \int_{0}^{P_0} q \frac{dp}{g}$$

where g is the gravitational acceleration constant (9.806 m/s), q is the specific humidity, dp is the difference between adjacent pressure levels (hPa).

Since the TCWV CDR-1 and CDR-2 are cloud screened over land, the daily outputs of the CMIP6 TCWV are also screened by cloud thresholds. Here data with cloud fraction less than 50% at all vertical levels over land and precipitation less than 0.001kg/m^2/s^2 are employed to compare with the CCI water vapour product.

Table 6-1: List of CMIP6 models.
The variables employed are hus: specific humidity; cl: cloud fraction; pr: precipitation; sftlf: land area fraction; wap: atmospheric vertical velocity

Institution	Model ID	Horizontal resolution	Frequency	Start-time	End-time
CCCma	CanESM5	2.81° * 2.81°	daily	1950-01	2014-12
CNRM-CERFACS	CNRM-CM6-1	1.41° * 1.41°	daily	1979-01	2014-12
	CNRM-ESM2-1	1.41° * 1.41°	daily	1979-01	2014-12
IPSL	IPSL-CM6A-LR	1.25° * 2.50°	daily	1979-01	2014-12
MPI-M	MPI-ESM1-2-HR	0.94° * 0.94°	daily	1979-01	2014-12
NCAR	CESM2	0.94° * 1.25°	daily	1950-01	2014-12
	CESM2-WACCM	0.94° * 1.25°	daily	1950-01	2014-12

6.2 ERA5 data

Total column water vapour from ERA5 with hourly frequency are firstly integrated into daily data to be included in this research as reference data. To compare the data under the same conditions, a land–sea mask is employed for land and ocean separation. Similar to CMIP6 data, only data with total cloud cover (tcc) less than 95% and total column cloud liquid water (tclw) less than 0.005 kg/m^2 over land, and data with total precipitation (tp) less than 0.001 m over ocean are used in this study.

6.3 TCWV and large-scale circulation

6.3.1 Description of the method

Changes in water vapour in the tropical region are important for studies on climate change impacts. However, regional variations are strong and a global look may smooth out all the patterns induced by the large-scale atmospheric circulation. Therefore, in this study, the atmospheric vertical velocity at 500 hPa (w_{500}) is used to decompose the tropical atmospheric into “bins” of dynamic motion, following the method put forth in Bony et al. (2004). In this framework, every dynamical regime is studied in light of its statistical weight within the tropics.

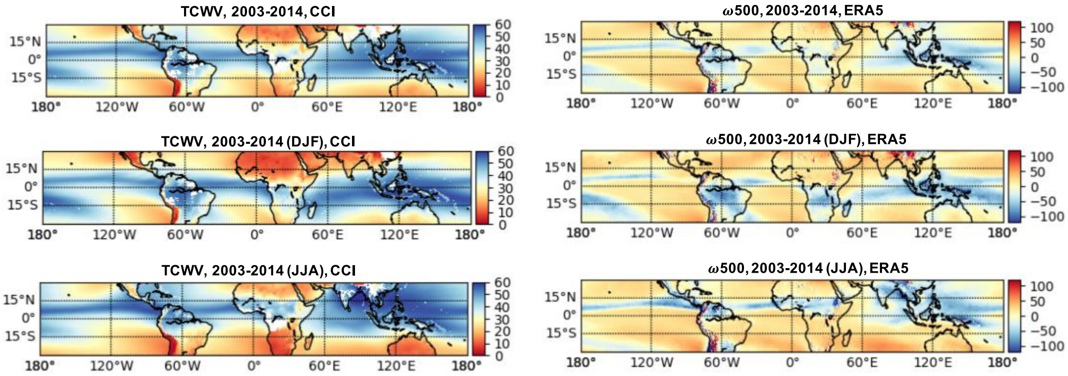

Figure 6-1: Distribution maps of total column water vapour obtained from CCI data record in the tropics (30°S–30°N) during 2003–2014 for the whole period, winter months (December, January, and February), and summer months (June, July, and August) (left panel), and their corresponding vertical velocity of w_{500} observed from ERA5.

Hence, for a given vertical velocity w_{500} (hPa/day) defined at a monthly scale, one can write:

$$\int_{-\infty}^{+\infty} P_{w500} dw_{500} = 1$$

Finite intervals of 10h Pa are used as a first attempt. The distribution maps of the TCWV from CCI data records and their corresponding vertical velocity of w_{500} from ERA5 are shown in Figure 6-2. The results show that the humid area is related with the ascending motion (negative value in w_{500}) and dry area is related with the subsiding motion (positive value in w_{500}).

As shown in Figure 6-2, the PDFs of the w_{500} from the CMIP6 models agrees well with the ERA5 data. Most of the w_{500} values are around 10–20 hPa/day over both land area and ocean area, which characterises the dominance of the clear-sky radiative cooling of the tropics.

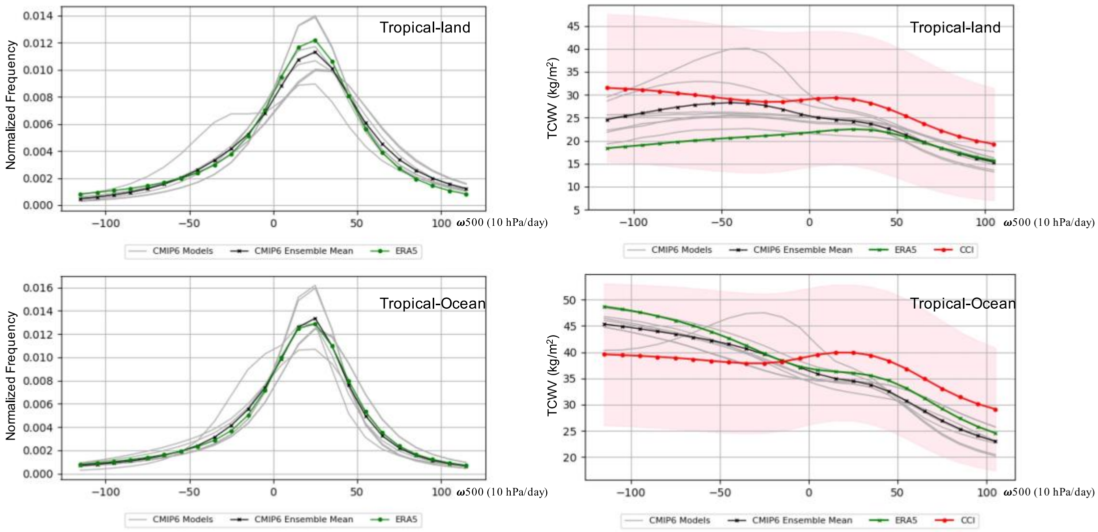

Figure 6-2: PDFs of w500 for CMIP6 models (grey lines), the ensemble mean of the models (black line), as well as ERA5 (green line). Here w_{500} from ERA5 is also employed as reference for the CCI data (left panel). Mean total column water vapour observed from the CMIP6 models (grey lines), the ensemble mean of CMIP6 (black line), ERA5 (green line), and CCI (red line) in different circulation regimes of w500. The shaded area in pink represents the ±σ of each bin in CDR-2.

Thanks to this decomposition, the variations of the TCWV can be studied with a dynamical perspective, looking at the behaviour of the TCWV for given bins of w_{500}, rather than with a fixed-box perspective. The CMIP6 models and the reanalysis results all show some differences with the WV_cci variables, but all are within the spread of the observation, indicating that the models could correctly represent the ascending motions and subsiding motions for large-scale circulation.

6.3.2 Analyses of the evolution according to dynamical regimes

We further decomposed the water vapour data into circulation regimes for each year to look into the details of the evolution of the water vapour. The results in Figure 6-3 show the variations of mean value of the total column water vapour for each circulation bins over the common 2004–2014 period in the tropical land region (30°S–30°N). Very different characteristics are observed for different data records. The tcwv from CCI data peak at -120 to -110 hPa/day bins, and it has a second peak in the tcwv value before 2009 at 20–30 hPa/day bins, while for the tcwv from ERA5, it peaks at 20–30 hPa/day bins. For the CMIP6 models, the high tcwv occurred at around -60 hPa/day bins.

This comparison provides an insight of the variation evolutions of the link between tcwv and the large-scale circulation over land area under clear-sky conditions. Despite the differences observed among the datasets, all the data records agree that the most positive w_{500} bins are associated with the driest troposphere (dark blue) while the most negative w_{500} bins are for the wettest troposphere (dark red).

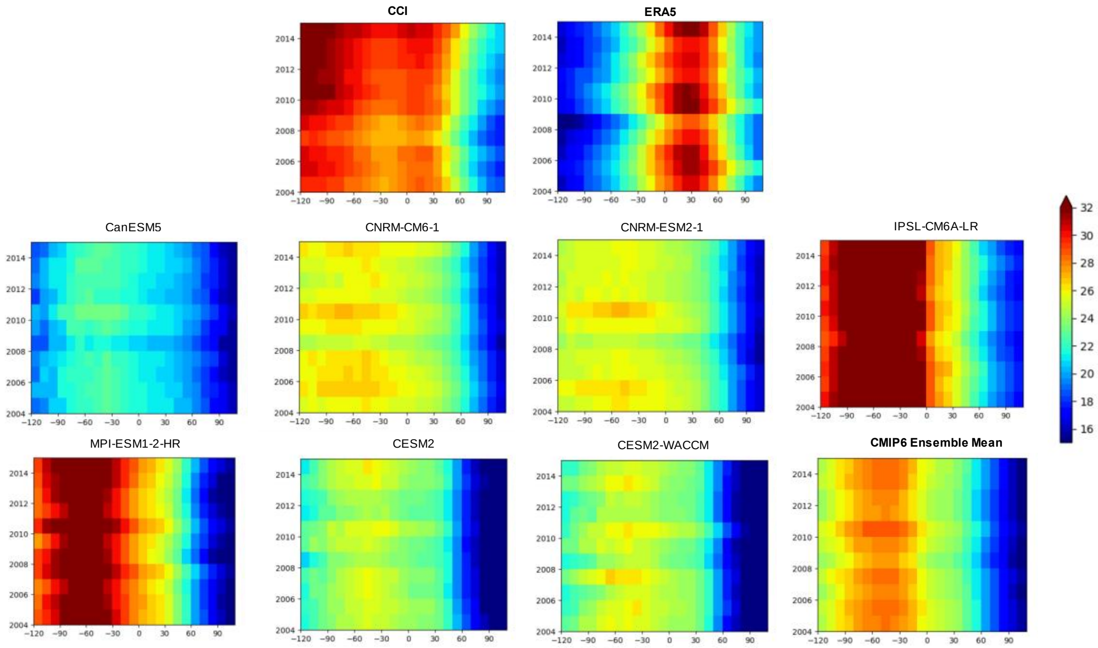
CCI ERA5 CanESM5 CNRM-CM6-1 CNRM-ESM2-1 IPSL-CM6A-LR MPI-ESM1-2-HR CESM2 CESM2-WACCM CMIP6 Ensemble Mean

Figure 6-3: Mean water vapour at each 10 hPa/day circulation regime over the land area of the tropics (30°S–30°N) for each year.

To analyse the evolution of circulation regimes, the mean water vapour value for the whole period of each data record at each bin are employed as the reference data to normalize the results. As is shown in Figure 6-4, dry anomalies in 2008 and wet anomalies in 2010 are observed for all data records. This possibly resulted from the La Niña events. In addition, a strong moistening trend is observed after 2009 from CCI data, while no significant moistening or desiccating trend is observed over the years in other data records.

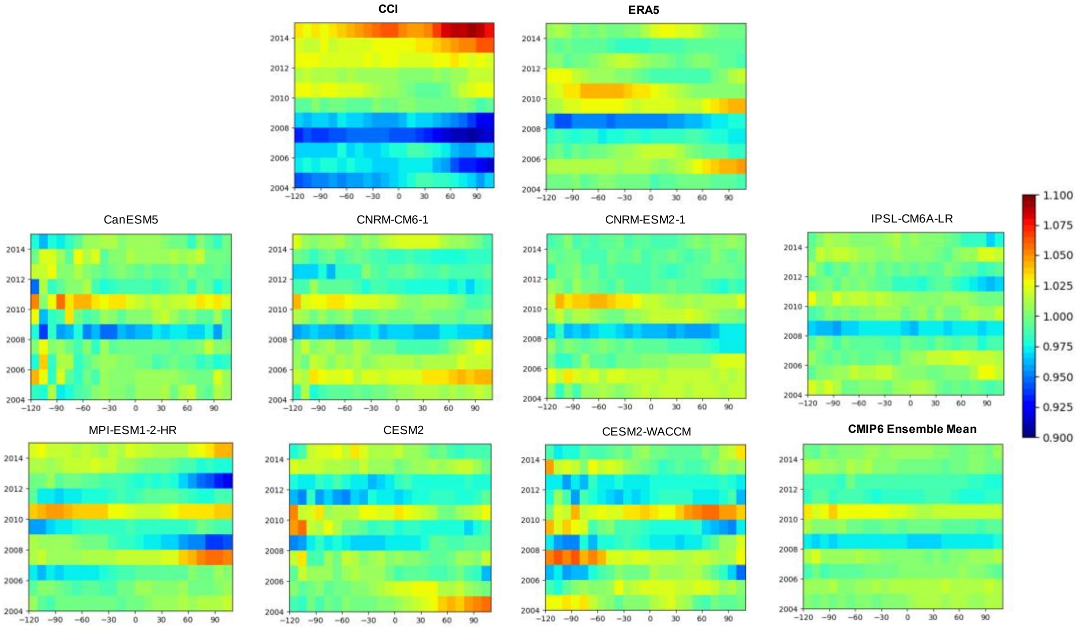

Figure 6-4: Normalised mean water vapour at each 10 hPa/day circulation regime over the land area of the tropics (30°S–30°N) for each year. The mean water vapour observed for the whole period of each data record are employed as the reference data.

The variations of mean value of the total column water vapour for each circulation bins over the common 2004–2014 period in the tropical ocean (30°S–30°N) are shown in Figure 6-5. Similar to the results observed over tropical land, the CCI data peak at -120 to -110 hPa/day bins, and it has a second peak in the tcwv value before 2009 at 20 – 30 hPa/day bins, while for the tcwv from ERA5 and most of the CMIP6 models (except for IPSL-CM6A-LR), the most moist value occurred at -120 to -110 hPa/day bins. For the IPSL-CM6A-LR model, the high tcwv occurred at around -30 hPa/day bins. In general, the data records perform more consistently over tropical ocean than over tropical land.

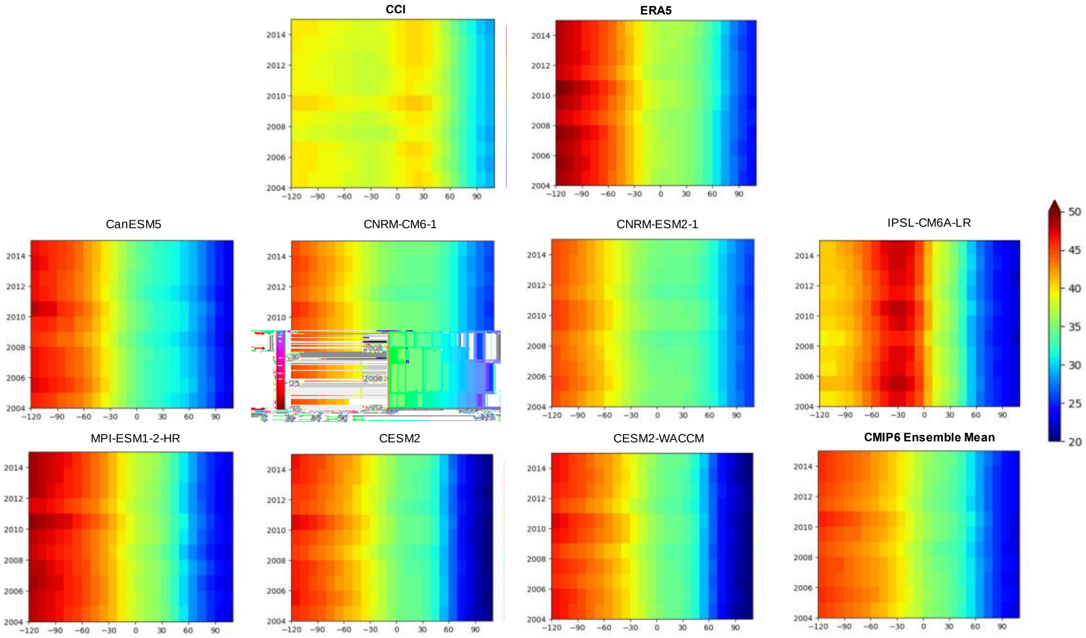

Figure 6-5: Mean water vapour at each 10 hPa/day circulation regime over the ocean area of the tropics (30°S–30°N) for each year.

Moreover, we also normalised the value by employing the mean tcwv observed for each circulation regime over the period 2004–2014 over ocean as the reference, to show the evolution of the water vapour in each circulation bin over the tropical ocean (30°S–30°N) in each year. The results in Figure 6-6 also show the dry anomalies in 2008 and wet anomalies in 2010 for all CMIP6 records and the ERA5 data, while for the CCI data, the dry anomalies are observed in 2007 and wet anomalies are in 2009.

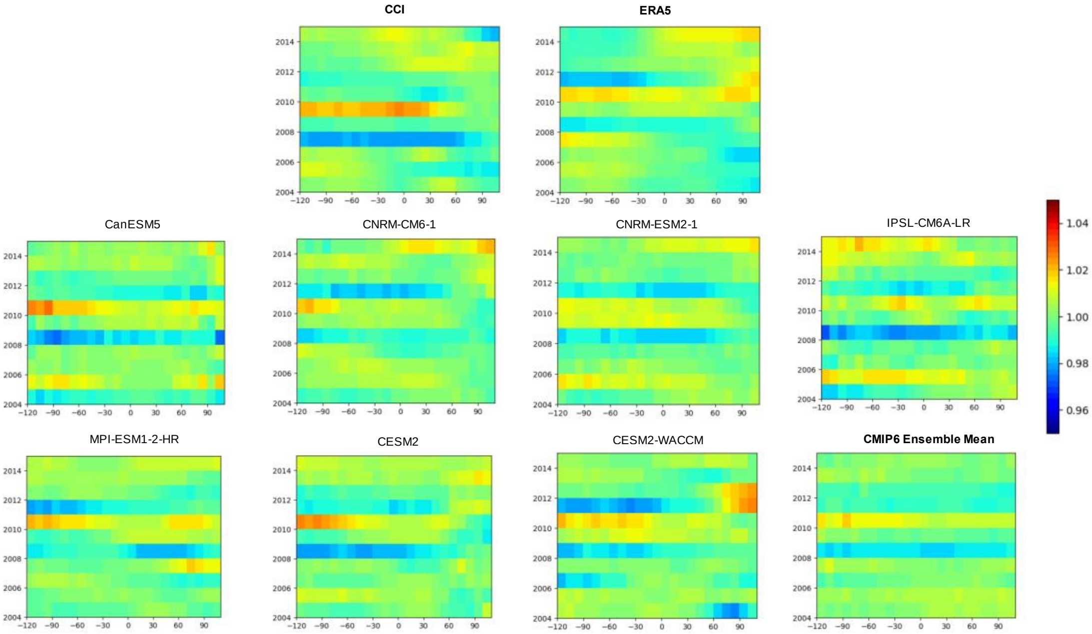

Figure 6-6: Normalised mean water vapour at each 10 hPa/day circulation regime over the ocean area of the tropics (30°S–30°N) for each year. The mean water vapour observed for the whole period of each data record are employed as the reference data.

6.4 Conclusions

The water vapour data obtained from the WV_cci project (CDR-1 and CDR-2), climate models (CMIP6 framework), and ERA5 are evaluated in terms of the representatives of the distribution and variation of tropospheric water vapour with respect to vertical velocity at 500 hPa. The results show that although there are differences observed among the CCI data, CMIP6 models, and the ERA5 data, all are within the spread of the observation, indicating that the models could correctly represent the large-scale circulation, which is that the humid area is related with the ascending motion (negative value in w_{500}) and dry area is related with the subsiding motion (positive value in w_{500}) over both tropical land and tropical ocean area.

7. SUMMARY OF THE WV_CCI USER WORKSHOP

The WV_cci User Workshop was successfully held in the afternoons of 14–16 June 2021, via zoom webinar (hosted by University of Reading) and with 100 registered participants and around 60 attendees each day. The workshop webpage (https://events.spacepole.be/event/122/timetable/#20210614.detailed), designed and hosted by BIRA), provides an overview of the agenda, participants, and presentations given at the workshop. A few specific comments are given in Appendix 2: Additional notes from Breakout Group sheets.

The aim of the workshop was to bring together the broader water vapour community, including those interested in the generation of water vapour CDRs and data users (such as climate modellers and NWP researchers) in order to discuss the most recent scientific applications and challenges in processing and using water vapour climate data records (CDRs). More specifically topics of the workshop included:

- Discuss challenges related to the generation of water vapour CDRs
- Show-case climate user applications of water vapour CDRs (with focus on WV_cci CDRs)
- Collect and update user requirements for atmospheric water vapour
- Present and discuss results from climate analysis, climate applications, and process studies using water vapour CDRs.

The three days were (roughly) dedicated to the following themes:

- **Day 1 –** WV_cci data products and user requirements
- **Day 2 –** Vertically resolved Water Vapour (VRWV) products and climate analysis
- **Day 3 –** Total Column WV (TCWV) products and climate analysis.

WV_cci presentations on **Day 1** included an overview of the CCI programme (Simon Pinnock) and introduction to the WV_cci (Michaela Hegglin), followed by two presentations on the TCWV products (Marc Schröder, Ulrike Falk) and VRWV products (Michaela Hegglin, Hao Ye). The session feedback provided helpful insights into the information data users would request when using the WV_cci datasets, including the clear-sky bias over land in the TCWV products (which was highlighted to be larger than potential long-term trends in the dataset) and the difficulty of the use of satellite measurement in the UTLS (the considered MIPAS observations, for example, only measure in cloud-free scenes, potentially leading to a sampling bias).

The presentations were followed by breakout groups which served the discussion of the user requirements in order to complete the user needs already collected at the start of the project (in the URD). Participants were able to choose the breakout group to join according to their interest in a particular CDR product (TCWV, VRWV-UTLS, and VRWV-stratosphere) WV_cci offers. The following seed questions for the discussion were given:

- How is your community currently defining user requirements for EO products? (surveys, experience, ...)
- How should user requirements ideally be established? (e.g., OSSEs for different requirements,...)
- What science questions should such a CDR be able to respond?
- Discuss the currently identified requirements for your climate data record (see https://climate.esa.int/en/projects/water-vapour/key-documents/), suggest updates, and provide evidence where requirements are not sufficient.

One key recommendation concerned the description of the TCWV CDR: the TCWV CDR is a daily product that combines data records over land and ocean. In both cases the diurnal cycle is not fully covered globally and not all atmospheric conditions are sampled. This causes an issue when comparing model output and the TCWV CDR since models are all skies and all-time. Therefore, there is a need for guidelines in the User Guide for *Dos and Don'ts* to apply CDRs.

For CDRs in general, more guidance is requested on how to use the uncertainty information when averaging on spatial and temporal scales, e.g. regional or zonal aggregation.

It was noted that a temporal coverage of approximately 15 years might be too short for climate change analysis.

Concerning user requirements, OSSEs could be defined to pin-point specific needs in terms of long-term trends. However, it has also been highlighted that many applications require different requirements that cannot be met with a single CDR.

On **Day 2,** the workshop continued with **Session 3** on available observational data in the UTLS and in the stratosphere:

- Rolf: JULIA: the Jülich airborne in-situ data base

The aircraft-based JULIA data record was introduced. Among others, it includes water vapour measurements up to a height of 21 km. The analysis of trends on basis of this data was not recommended.

- Rohs: IAGOS water vapour and RH_ice products

Also IAGOS is an aircraft based data record of among others water vapour and is based on MOZAIC. It covers the period 1994–present and a trend analysis does not exhibit significant trends.

- Ghysels-Dubois: STRATEOLE 2 balloon observations in the tropics

This data record relies on long-term balloon campaigns and measures in the TTL/lower equatorial stratosphere. A bias relative to data from MLS was observed. In early 2022 there will be a hygrometer intercomparison campaign.

- Davis: SWOOSH: a long-term data base for climate studies

SWOOSH combines various satellite-based observations into a stratospheric water vapour profile data record using MLS as reference. It starts in 1984 and is available in v2.6 and v2.7 beta. The product does not contain uncertainty correlations.

- Schneider: Water vapour isotopologue observations from space

The retrieval and analysis of water vapour isotopologues from IASI (MUSICA) and TROPOMI were presented. Such analysis is not possible with water vapour data alone and the combined utilisation allows extracting vertical information as well.

Day 2 moved on with presentations on VRWV H_2O observations. Some take home messages from **Session 4** include:

- Nielsen et al: Retrieval of high VR trop. specific humidity from RO

The tropospheric specific humidity and temperature retrieved from radio occultations using a 1D-Var model, shows good specific humidity accuracy and vertical resolution in the mid-troposphere. Comparisons with GRUAN radiosonde profiles show that the estimated uncertainties in specific humidity and temperature in RO are similar to the uncertainties from GRUAN.

- Gleisner et al.: ROM SAF humidity climate data records based on RO

The ROM SAF CDR data (specific humidity up to 12 km and temperature in both troposphere and stratosphere) includes a special variable in specific humidity as “a priori fraction” to show the estimated impacts from observations. The statistical analysis shows that the specific humidity variability is dominated by ENSO signals. The specific humidity data starting from 2006 is long enough for climatic trend research.

- Willet et al: HadISDH surface humidity

The HadISDH dataset, a global surface humidity product from *in situ* observations from land stations and ships, shows an increasing specific humidity trend and a decreasing relative humidity trend over both land and ocean, which are similar to reanalyses and TCWV. This dataset is long enough (from 1973 onward) to compare with reanalyses and historical runs from climate models (CMIP5/6).

There are still big gaps and difficulties to get a combined VRWV data. The specific humidity in troposphere could be potentially used to compare with RAL IMS in the mid-and low-troposphere as IMS is used in CDR-4 in the troposphere. Surface humidity data may have some potential connections with CDR-1&2.

Session 5 focussed on WV_cci internal analysis of TCWV CDRs.

- Ebell et al: Systematic assessment of WV products in the Arctic

Various satellite-based and reanalysis data records were intercompared over the Arctic region. Results indicate good quality for IASI TCWV data while GOME products fairly strongly underestimate TCWV. In presence of sea-ice largest differences are observed between the data records.

- Jorge Eiras-Barca et al: Contribution to atmospheric moisture transport (WV_cci)

CDR-2 was compared with reanalysis and both products exhibit reasonable agreement. CDR-2 cannot be used for a full analysis of atmospheric rivers due to the lack of vertically resolved data.

- Ramos et al.: The use of WV products in Atmospheric Rivers Science

This presentation highlighted the need of the use of novel long-term TCWV climatologies or/and water vapour profiles in order to better understand the genesis and dynamics of atmospheric rivers. An interest in utilising CDR-2 was expressed.

Day 2 ended with a discussion on critical observations gaps (e.g. in terms of resolution, coverage, quality, (potential) sensor loss), how these could be addressed, and what process studies would lead to better knowledge of the role of water vapour in the climate system. It was briefly discussed that a critical gap might occur between currently flying microwave imagers which are all beyond expected life-time and newly launched missions with microwave imagers on board (i.e. EPS-SG, GOSAT-GW). Also, a critical gap might occur for limb sounding missions. Again, the currently flying missions are beyond life-time and new missions are not committed yet. Potential missions might come from ESA and Canada. If a gap occurs ground-based observations might be used to fill the gap. It was generally noted that the validation in the UTLS can be considered as gap.

Day 3 was the final day of the workshop. **Session 6** discussed total column water vapour observations and climate analysis with the following presentation summaries:

- Falk et al.: TCWV: trends, variability & theoretical expectation (WV_cci)

Presentation of ongoing results from the ESA water vapour CCI project, examining trends of TCWV from CDR-1 and 2, AIRS, ERA5 and merged microwave products. The analysis is broken down into global ice-free ocean and land regions between ±60° (latitude), and examined for the common time period between the records. Regression against surface air temperature from the H2020 EUSTRACE project, as well as land and sea surface temperatures from the ESA CCI program has also performed. The work is still ongoing, with the final results expected in August (2021).

- Borger et al.: Analysis of global trends of TCWV from OMI observations

This study presents analysis of TCWV trends from the Ozone Monitoring Instrument (OMI). TCWV is retrieved from the blue region in the visible spectrum (400 nm) using the Differential Optical Absorption Spectroscopy (DOAS) technique. This algorithm has already been successfully applied to TROPOMI, with potential for future sensors also. Inter-comparisons to SSM/I TCWV (over ocean) showed around 3% wet bias with some inter-annual variability. Similar results were also seen for comparisons to ERA5 over ocean, with a wet bias of 5% observed. However, over land surfaces this increases to an 11% wet bias relative to ERA5, with most overestimation coming from the Amazon basin. Further work was also presented on work with trends, with no detectable Clausius–Clapeyron response.

- Küchler et al.: Comparison of Sentinel-5P TCWV from different algorithms

This work focused on the comparison of three different TROPOMI TCWV products, i) AMC-DOAS, ii) MPIC, and iii) SRON to demonstrate the advantage of multiple products from the same sensor. These products also make use of different parts of the TROPOMI spectra for water vapour information. An overview of the products was presented, with a focus on differences in quality and cloud filtering. Intercomparison of the products is given by scatter plots, time series, and monthly mean difference map plots. Overall, there is a good agreement between the products (within 2 kg/m^2) and with reanalysis. However, complex structures are present in the difference maps.

- Radice et al.: Novel assessment of model relative humidity with satellite probabilistic estimates

This study focuses on using retrievals of relative humidity (RH) from the SAPHIR microwave sounder to assess NWP forecasts from the ARPEGE model, operated by Météo-France. Rather than bulk metrics (e.g. bias, correlation etc), a novel approach is used whereby the model forecast is projected onto PDF information from the RH retrieval. Transforming the PDF to a CDF then allows for the probability that forecast is higher/lower than the true RH to be determined. This new method highlighted regions where the forecast diverge from the satellite RH which were not visible when comparing the differences directly. Overall, ARPEGE was found to overestimate more frequently than underestimate the RH outside of the 0.25-0.75 confidence interval.

- Castelli et al.: AIRWAVE-TCWV from TIR dual view ATSR-like instruments

This final presentation of the session discussed the AIRWAVE algorithm and the application to ATSR-like instruments that operate in the infrared. The AIRWAVE algorithm has been developed within the ESA long-term preservation of ATSR framework. While these instruments were designed to measure surface temperature, the dual-view aspect which is used for atmospheric correction can be exploited to provide TCWV information. Validation of version 1 of the algorithm showed biases of 2.43 kg/m^2 relative to island based radiosondes, and 2.11 kg/m^2 relative to SSM/I. For updates in version 2, these biases reduced to 0.19 kg/m^2 and 0.02 kg/m^2 respectively. Examples of applications using the v1 and v2 datasets were also shown (ITCZ displacement trends and lee wave detection respectively). Ongoing work includes the application of the AIRWAVE algorithm to the SLSTR instruments.

The second session of the third day addressed TCWV, focusing on model intercomparisons.

- He et al., from the LATMOS group

Sought to discern between the dynamic and thermodynamic components of TCWV variations, making more explicit the link between the TCWV and large-scale circulation. They addressed this issue by jointly analysing CDR-2 from WV_cci with

ERA5 and CMIP6 outputs. Among other interesting results, they found a moistening trend observed in CCI data, a dry bias in ERA5 over land, and that all CMIP6 models vary within the standard deviation of the CDR-2 in each circulation bin of vertical velocity at 500 hPa.

- Richard P. Allan from the UoR evaluated WV changes in CMIP6 simulations

They found that WV changes are broadly captured by CMIP6 models and observing systems and reported suppressed WV trend in the atmospheric model intercomparison project (AMIP) vs historical.

- Lauer et al., from the DLR

Provided an evaluation of the CMIP6 with the CDR-2 using the ESMValTool. Among other results, they reported that, when talking about TCWV, the multi-model mean climatology is quite close to observations. Also, the seasonal cycle amplitude seems to be overestimated in the Tropics and underestimated over North America and Europe.

- William Ingram, from the Met Office Hadley Centre

Analysed the effects of model resolutions in the WV validation in a GCM. He stated that most GCMs have climate sensitivities above the accepted uncertainty ranges.

- Trent et al. from the U. of Leicester

Addressed the issue of the water vapour residence time (WVRT) from observational and AMIP ensembles. They reported differences up to 0.4 days in WVRT between models and observations and some disparities in TCWV over strong convective regions and in NH summer, being the latter more likely linked to meridional transport in models.

Final discussions on climate analysis, applications & process studies raised the following: Process studies leading to a better knowledge of the role of water vapour in the climate system could be pursued, e.g. the role of entrainment/detrainment on convective scales. Other topics include a close analysis of the homogeneity of the products and interproduct consistency. An improved parameterisation of the clear-sky OLR using satellite data would be beneficial as well.

Finally the organisers thanked all participants for valuable contributions via presentations and discussions.

8. DEDICATED USER FEEDBACK ON WV_CCI CDRS

8.1 Introduction and usage

The WV_cci datasets comprise four CDRs (see also section 1.4):

- CDR-1: gridded monthly and daily means of TCWV in units of kg/m^2 that cover the global land areas with a spatial resolution of 0.05°. It covers the period July 2002 to December 2017.
- CDR-2: gridded monthly and daily means of TCWV in units of kg/m^2 with global coverage and a spatial resolution of 0.05° / 0.5°. It covers the period July 2002 to December 2017.
- CDR-3 contains the vertically resolved water vapour ECV in units of ppmv (volume mixing ratio) as zonal monthly means on the SPARC Data Initiative latitude/pressure level grid. It covers the vertical range between 250 hPa and 1 hPa, and the time period 1985 to December 2019.
- CDR-4 consists of three-dimensional vertically resolved monthly mean water vapour data (in ppmv) with a spatial resolution of 100 km, covering the troposphere and lower stratosphere.

The final versions of CDR-1 and CDR-2 are v3.1 and are available to CCI and on request since February 2021. Results from project internal analysis are summarised in this report (Section 2 to Section 6) and in He et al. (2022) and Eiras-Barca et al. (2022). At the time of writing, CDR-3 and CDR-4 were not available in final form. Nonetheless, a pre-final version of CDR-3 was available for project-internal scientific analysis (see Section 4).

Beyond WV_cci project partners the following institutions requested data access to CDR-1 and CDR-2:

- DLR, Germany
- University of Bremen, Germany
- University of New Brunswick, Canada
- University of Lisbon, Portugal
- MPI-C, Germany
- DWD, Germany
- Planetary Visions Limited, UK

The project is aware of the following WV_cci external publication which utilises WV_cci data:

- Lauer et al. (2022): They assessed the improvement of CMIP6 relative CMIP5 model output using CDR-2 from WV_cci and cloud data records from Clouds_cci.

8.2 Feedback

The summary of feedback from users of WV_cci datasets is based on the following:

- Email exchange between project and WV_cci data record users
- Talk at AR3 on CDR-3 analysis
- Presentations at the WV_cci user workshop.

The feedback from emails relies on three users and is summarised as follows:

- In comparisons to other data records a contrast in results over ocean and land was observed.
- The contrast in uncertainty magnitude between land and ocean was noted.
- The data was partly used independent of its sampling characteristics, i.e. it was treated as all-sky data.

The key feedback is the contrast in different characteristics of the product over land and ocean. Such a contrast can be expected given the nature of CDR-2, as documented in PVIR and PUG. However, CDR-2 was provided to users at an early project stage, with the main motivation to allow timely analysis of the data. At that time PVIR and PUG were not available.

Results from the analysis of CDR-3 were presented at the Annual Review Meeting 3 on 26 and 27 August 2021. The presentation concluded with the following statements:

- Insignificant differences in amplitude and phase of (inter)annual cycles
- Significant difference in multi-annual mean
- Structure and sign of trends generally agree well
- Largest disagreement in 1998–2003 period
- Trends since 2004 depend on Aura MLS version and data sets included.

It was concluded that CDR-3 includes more sensors and more information compared with other available CDRs.

The WV_cci User Workshop was held in the afternoons of 14–16 June 2021. A summary and details from discussions are given in Section 7 and in Appendix 2, respectively. Here, we focus on presentations given by users and the user community with explicit feedback in relation to WV_cci data records. The talks given by the following first authors form the basis for the summary given below: Gimeno Presa, Ramos, He, Lauer, Allan, and Ingram.

The feedback is summarised as follows:

General:

- Gaps, in particular in space, require additional efforts in comparison exercises and might impact the conclusions.
- Despite the significant progress in the generation of satellite-based CDRs a comparison to multiple CDRs is still recommended.
- Products with sub-daily resolution are required for process studies.
- Multi-layer tropospheric data records are required for various applications, as for example for the analysis of atmospheric rivers.

TCWV:

- Relative to ERA5 and a subset of CMIP6 models CDR-1 exhibits a fairly strong increase in anomalies over the tropical land.

It can be concluded that higher resolutions would be supportive for additional or more advanced analysis. Even though the high stability of the TCWV product was demonstrated it seems advisable to reassess its stability in the future.

APPENDIX 1: REFERENCES

Algarra, I., Eiras-Barca, J., Nieto, R., & Gimeno, L. (2019a). Global climatology of nocturnal low-level jets and associated moisture sources and sinks. Atmospheric Research, 229, 39-59.

Algarra, I., Eiras-Barca, J., Miguez-Macho, G., Nieto, R., & Gimeno, L. (2019b). On the assessment of the moisture transport by the Great Plains low-level jet. Earth System Dynamics, 10(1), 107-119.

ATBD v2.1 (2020) Algorithm Theoretical Basis Document, Part 3 - Merged CDR-3 and CDR-4 products. ESA/ECSAT, WV_cci Phase One, Ref: CCIWV.REP.022, version 1.1, 13 October 2020.

Algarra, I., Nieto, R., Ramos, A. M., Eiras-Barca, J., Trigo, R. M., & Gimeno, L. (2020). Significant increase of global anomalous moisture uptake feeding landfalling Atmospheric Rivers. Nature communications, 11(1), 1-7.DARD (2021): Data access requirement document. ESA/ECSAT, WV_cci Phase One, Ref: CCIWV.REP.003, version 3.1, 24 March 2021.

Bony, S., J.-L. Dufresne, H. LeTreut, J.-J. Morcrette, and C. Senior (2004), On dynamic and thermodynamic components of cloud changes, Clim. Dyn., 22, 71–86.

Byrne, M. P. & O'Gorman, P. A., 2013: Link between land-ocean warming contrast and surface relative humidities in simulations with coupled climate models. Geophysical Research Letters 40, 5223-5227

Byrne, M. P. & O'Gorman, P. A., 2016: Understanding decreases in land relative humidity with global warming: conceptual model and GCM simulations. Journal of Climate 29, 9045-9061

DARD v3.2 (2021) Data Access Requirement Document. ESA/ECSAT, WV_cci Phase One, Ref: CCIWV.REP.003, version 3.2, 27 July 2021.

Davis, S. M., Rosenlof, K. H., Hassler, B., Hurst, D. F., Read, W. G., Vömel, H., Selkirk, H., Fujiwara, M., and Damadeo, R.: The Stratospheric Water and Ozone Satellite Homogenized (SWOOSH) database: a long-term database for climate studies, Earth Syst. Sci. Data, 8, 461–490, https://doi.org/10.5194/essd-8-461-2016, 2016.

Dessler, A.E. & Davis, S.M. Trends in tropospheric humidity from reanalysis systems. J. Geophys. Res. 2010, 115, D19127.

Dessler, A. E., Schoeberl, M. R., Wang, T., Davis, S. M., Rosenlof, K. H., and Vernier, J.-P.: Variations of stratospheric water vapor over the past three decades, J. Geophys. Res. Atmos., 119, 12588-12598, doi:10.1002/2014JD021712, 2014.

Diallo, M., Riese, M., Birner, T., Konopka, P., Müller, R., Hegglin, M. I., Santee, M. L., Baldwin, M., Legras, B., and Ploeger, F.: Response of stratospheric water vapor and ozone to the unusual timing of El Niño and the QBO disruption in 2015–2016, Atmos. Chem. Phys., 18, 13055–13073, https://doi.org/10.5194/acp-18-13055-2018, 2018.

Eiras-Barca, J., Dominguez, F., Hu, H., Garaboa-Paz, D., & Miguez-Macho, G. (2017). Evaluation of the moisture sources in two extreme landfalling atmospheric river events using an Eulerian WRF tracers tool. Earth System Dynamics, 8(4), 1247-1261.

Eiras-Barca, J., I. Algarra, R. Nieto, M. Schröder, M. Hegglin, and L. Gimeno, 2022: Analysis of the main sources associated with moisture transport events with the new ESA CCI/CM SAF total column water vapour climate data record. Under review at QJRMS.

Fetzer, E. J., B. H. Lambrigtsen, A. Eldering, H. H. Aumann, and M. T. Chahine (2006), Biases in total precipitable water vapor climatologies from atmospheric infrared sounder and advanced microwave scanning radiometer, J. Geophys. Res., 111, D09S16, doi:10.1029/2005JD006598.

Froidevaux, L., Anderson, J., Wang, H.-J., Fuller, R. A., Schwartz, M. J., Santee, M. L., Livesey, N. J., Pumphrey, H. C., Bernath, P. F., Russell III, J. M., and McCormick, M. P.: Global OZone Chemistry And Related trace gas Data records for the Stratosphere (GOZCARDS): methodology and sample results with a focus on HCl, H2O, and O3, Atmos. Chem. Phys., 15, 10471–10507, https://doi.org/10.5194/acp-15-10471-2015, 2015.

GCOS, The Global Climate Observing System for Climate: Implementation Plan. WMO GCOS-200, 341 pp., 2016. Available at https://library.wmo.int/doc_num.php?explnum_id=3417

Gimeno, L., Nieto, R., Vázquez, M., & Lavers, D. A. (2014). Atmospheric rivers: A mini-review. Frontiers in Earth Science, 2.

Gimeno, Luis, Francina Dominguez, Raquel Nieto, Ricardo Trigo, Anita Drumond, Chris J.C. Reason, Andréa S. Taschetto, Alexandre M. Ramos, Ramesh Kumar, José Marengo, 2016: Major Mechanisms of Atmospheric Moisture Transport and Their Role in Extreme Precipitation Events. Annual Review of Environment and Resources 2016 41:1, 117-141

Good, E., 2016. An in situ-based analysis of the relationship between land surface ‘skin’ and screen-level air temperatures. Journal of Geophysical Research-Atmospheres, Volume 121, Issue 15, Pages: 8801–8819. doi.org/10.1002/2016JD025318.

He, J., Brogniez, H., and Picon, L. (2022) Evaluation of tropical water vapour from CMIP6 GCMs using the ESA CCI "Water Vapour" climate data records, Atmos. Chem. Phys. Discuss. [preprint], https://doi.org/10.5194/acp-2021-976, in review.

Hegglin, M.I., Plummer, D.A., Shepherd, T.G., Scinocca, J.F., Anderson, J., Froidevaux, L., Funke, B., Hurst, D., Rozanov, A., Urban, J. and von Clarmann, T. (2014): Vertical structure of stratospheric water vapour trends derived from merged satellite data. Nature geoscience, 7(10), p.768.

Held, I. M., & Soden, B. J. (2006). Robust responses of the hydrological cycle to global warming. Journal of climate, 19(21), 5686-5699.

Hersbach, H., Bell, B., Berrisford, P., Hirahara, S., Horányi, A., Muñoz-Sabater, J., et al. and Simmons, A. (2020). The ERA5 global reanalysis. Quarterly Journal of the Royal Meteorological Society, doi:10.1002/qj.3803.

Hurst, D. F., Oltmans, S. J., Vömel, H., Rosenlof, K. H., Davis, S. M., Ray, E. A., Hall, E. G., and Jordan, A. F.: Stratospheric water vapor trends over Boulder, Colorado: Analysis of the 30 year Boulder record, J. Geophys. Res., 116, D02306, doi:10.1029/2010JD015065, 2011.

Hurst, D. F., Read, W. G., Vömel, H., Selkirk, H. B., Rosenlof, K. H., Davis, S. M., Hall, E. G., Jordan, A. F., and Oltmans, S. J.: Recent divergences in stratospheric water vapor measurements by frost point hygrometers and the Aura Microwave Limb Sounder, Atmos. Meas. Tech., 9, 4447–4457, https://doi.org/10.5194/amt-9-4447-2016, 2016.

Hyland, R. W., and A. Wexler (1983), Formulations for the thermodynamic properties of the saturated phases of H2O from 173.15 K to 473.15 K, ASHRAE Trans., 89(2A), 500–519.

IPCC, 2013: Climate Change 2013: The Physical Science Basis. Contribution of Working Group I to the Fifth Assessment Report of the Intergovernmental Panel on Climate Change [Stocker, T.F., D. Qin, G.-K. Plattner, M. Tignor, S.K. Allen, J. Boschung, A. Nauels, Y. Xia, V. Bex and P.M. Midgley (eds.)]. Cambridge University Press, Cambridge, United Kingdom and New York, NY, USA, 1535 pp.

IPCC, 2018: Global Warming of 1.5°C. An IPCC Special Report on the impacts of global warming of 1.5°C above pre-industrial levels and related global greenhouse gas emission pathways, in the context of strengthening the global response to the threat of climate change, sustainable development, and efforts to eradicate poverty [Masson-Delmotte, V., P. Zhai, H.-O. Pörtner, D. Roberts, J. Skea, P.R. Shukla, A. Pirani, W. Moufouma-Okia, C. Péan, R. Pidcock, S. Connors, J.B.R. Matthews, Y. Chen, X. Zhou, M.I. Gomis, E. Lonnoy, T. Maycock, M. Tignor, and T. Waterfield (eds.)]

Lauer, A., L. Bock, B. Hassler, M. Schröder, M. Stengel, 2022: Cloud climatologies from global climate models – a comparison of CMIP5 and CMIP6 models with satellite data. Submitted to J. Geophys. Res.

Livesey, N. J., Read, W. G., Froidevaux, L., Lambert, A., Santee, M. L., Schwartz, M. J., Millán, L. F., Jarnot, R. F., Wagner, P. A., Hurst, D. F., Walker, K. A., Sheese, P. E., and Nedoluha, G. E.: Investigation and amelioration of long-term instrumental drifts in water vapor and nitrous oxide measurements from the Aura Microwave Limb Sounder (MLS) and their implications for studies of variability and trends, Atmos. Chem. Phys. Discuss. [preprint], https://doi.org/10.5194/acp-2021-440, in review, 2021.

Lossow, S., Khosrawi, F., Nedoluha, G. E., Azam, F., Bramstedt, K., Burrows, John. P., Dinelli, B. M., Eriksson, P., Espy, P. J., García-Comas, M., Gille, J. C., Kiefer, M., Noël, S., Raspollini, P., Read, W. G., Rosenlof, K. H., Rozanov, A., Sioris, C. E., Stiller, G. P., Walker, K. A., and Weigel, K.: The SPARC water vapour assessment II: comparison of annual, semi-annual and quasi-biennial variations in stratospheric and lower mesospheric water vapour observed from satellites, Atmos. Meas. Tech., 10, 1111–1137, https://doi.org/10.5194/amt-10-1111-2017, 2017a.

Lossow, S., Garny, H., and Jöckel, P.: An “island” in the stratosphere – on the enhanced annual variation of water vapour in the middle and upper stratosphere in the southern tropics and subtropics, Atmos. Chem. Phys., 17, 11521–11539, https://doi.org/10.5194/acp-17-11521-2017, 2017b.

Lossow, S., Hurst, D. F., Rosenlof, K. H., Stiller, G. P., von Clarmann, T., Brinkop, S., Dameris, M., Jöckel, P., Kinnison, D. E., Plieninger, J., Plummer, D. A., Ploeger, F., Read, W. G., Remsberg, E. E., Russell, J. M., and Tao, M.: Trend differences in lower stratospheric water vapour between Boulder and the zonal mean and their role in understanding fundamental observational discrepancies, Atmos. Chem. Phys., 18, 8331–8351, https://doi.org/10.5194/acp-18-8331-2018, 2018.

Mears, C.A.; Santer, B.D.; Wentz, F.J.; Taylor, K.E.; Wehner, M.F. Relationship between temperature and precipitable water changes over tropical oceans. Geophys. Res. Lett., 2007, 34, L24709.

Mieruch, S.; Schröder, M.; Noel, S.; Schulz, J. Comparison of decadal global water vapour changes derived from independent satellite time series. J. Geophys. Res. Atmos. 2014, 119.

Millán, L. F., Lebsock, M. D., and Teixeira, J.: Variability of bulk water vapor content in the marine cloudy boundary layers from microwave and near-infrared imagery, Atmos. Chem. Phys., 19, 8491–8502, https://doi.org/10.5194/acp-19-8491-2019, 2019.

O’Gorman, P. A., & Muller, C. J. (2010). How closely do changes in surface and column water vapor follow Clausius–Clapeyron scaling in climate change simulations?. Environmental Research Letters, 5(2), 025207.

PSD (2021): Product Specification Document. ESA/ECSAT, WV_cci Phase One, Ref: CCIWV.REP.002, version 3.2, 27 July 2021.

PUG (2021) Product User Guide. ESA/ECSAT, WV_cci Phase One, Ref: CCIWV.REP.017, version 2.0, 25 August 2021

PVIR (2021): Product Validation and Intercomparison Report Part 1: CDR-1 & CDR-2. ESA/ECSAT, WV_cci Phase One, Ref: CCIWV.REP.016, version 2.1, 30 September 2021.

PVP (2021): Product Validation Plan. ESA/ECSAT, WV_cci Phase One, Ref: CCIWV.REP.008, version 3.2, 29 July 2021.

Randel, W., & Park, M.: Diagnosing observed stratospheric water vapor relationships to the cold point tropical tropopause. Journal of Geophysical Research: Atmospheres, 124, 7018–7033. https://doi.org/10.1029/2019JD030648, 2019.

Rayner, N. A., Auchmann, R., Bessembinder, J., Brönnimann, S., Brugnara, Y., Capponi, F., et al. (2020). The EUSTACE project: Delivering global daily information on surface air temperature. Bulletin of the American Meteorological Society, E1924–E1947, https://doi.org/10.1175/BAMS-D-19-0095.1

Schieferdecker, T., Lossow, S., Stiller, G. P., and von Clarmann, T.: Is there a solar signal in lower stratospheric water vapour?, Atmos. Chem. Phys., 15, 9851–9863, https://doi.org/10.5194/acp-15-9851-2015, 2015.

Schröder, M.; Lockhoff, M.; Forsythe, J.; Cronk, H.; Vonder Haar, T.H.; Bennartz, R. The GEWEX water vapor assessment (G-VAP)—Results from the trend and homogeneity analysis. J. Appl. Meteor. Clim. 2016, 55, 1633–1649.

Schröder, M.; Lockhoff, M.; Shi, L.; August, T.; Bennartz, R.; Borbas, E.; Brogniez, H.; Calbet, X.; Crewell, S.; Eikenberg, S.; et al. GEWEX Water Vapor Assessment (G-VAP); WCRP Report 16/2017;World Climate Research Programme (WCRP): Geneva, Switzerland, 2017; 216p, Available online: https://www.wcrp-climate.org/resources/wcrp-publications (accessed on 24 January 2019).

Schröder, M., Lockhoff, M., Fell, F., Forsythe, J., Trent, T., Bennartz, R., Borbas, E., Bosilovich, M. G., Castelli, E., Hersbach, H., Kachi, M., Kobayashi, S., Kursinski, E. R., Loyola, D., Mears, C., Preusker, R., Rossow, W. B., and Saha, S.: The GEWEX Water Vapor Assessment archive of water vapour products from satellite observations and reanalyses, Earth Syst. Sci. Data, 10, 1093-1117, https://doi.org/10.5194/essd-10-1093-2018, 2018.

Schröder, M.; Lockhoff, M.; Shi, L.; August, T.; Bennartz, R.; Brogniez, H.; Calbet, X.; Fell, F.; Forsythe, J.; Gambacorta, A.; Ho, S.-p.; Kursinski, E.R.; Reale, A.; Trent, T.; Yang, Q. The GEWEX Water Vapor Assessment: Overview and Introduction to Results and Recommendations. Remote Sens. 2019, 11, 251. https://doi.org/10.3390/rs11030251.

Sherwood, S. C., R. Roca, T. M. Weckwerth, and N. G. Andronova (2010), Tropospheric water vapor, convection, and climate/ Rev. Geophys.,48, RG2001, doi:10.1029/2009RG000301.

Shi, L., C. J. Schreck III, M. Schröder, 2018: Assessing the pattern differences between satellite-observed upper tropospheric humidity and total column water vapor during major El Niño events. Remote Sens. 2018, 10, 1188; https://doi.org/10.3390/rs10081188.

Soden, B. J., Jackson, D. L., Ramaswamy, V., Schwarzkopf, M. D., & Huang, X. (2005). The radiative signature of upper tropospheric moistening. Science, 310(5749), 841-844.

Sohn, B.-J., and R. Bennartz (2008), Contribution of water vapor to observational estimates of longwave cloud radiative forcing, J. Geophys. Res., 113, D20107, doi:10.1029/2008JD010053.

SPARC, 2017: The SPARC Data Initiative: Assessment of stratospheric trace gas and aerosol climatologies from satellite limb sounders. By M. I. Hegglin and S. Tegtmeier (eds.), SPARC

Report No. 8, WCRP-5/2017, available at www.sparc-climate.org/publications/sparc-reports/sparc-report-no8

Stephens, G. L., Hakuba, M. Z., Webb, M. J., Lebsock, M., Yue, Q., Kahn, B. H., et al. (2018). Regional intensification of the tropical hydrological cycle during ENSO. Geophysical Research Letters, 45, 4361–4370. https://doi.org/10.1029/2018GL077598

Stubenrauch, C., W. B. Rossow, and S. Kinne, 2012: Assessment of global cloud datasets from satellites: A project of the World Climate Research Programme Global Energy and Water Cycle Experiment (GEWEX) Radiation Panel. WCRP Rep. 23/2012, 176 pp. [Available online at www.wcrp-climate.org/documents/GEWEX_Cloud_Assessment_2012.pdf.]

Trenberth, K. E., J. Fasullo, and L. Smith, 2005: Trends and variability in column- integrated atmospheric water vapour. Climate Dyn., 24, 741–758, doi:10.1007/s00382-005-0017-4.

URD (2021) User Requirements Document. ESA/ECSAT, WV_cci Phase One, Ref: CCIWV.REP.001, version 3.0, 11 February 2021.

Weatherhead, E. C., et al. (1998), Factors affecting the detection of trends: Statistical considerations and applications to environmental data, J. Geophys. Res., 103(D14), 17,149–17,161, doi:10.1029/98JD00995.

Wentz, F.J.; Schabel, M.C. Precise climate monitoring using complementary satellite data sets. Nature 2000, 403, 414–416.

Whiteman, D. N., K. C. Vermeesch, L. D. Oman, and E. C. Weatherhead (2011), The relative importance of random error and observation frequency in detecting trends in upper tropospheric water vapor, J. Geophys. Res., 116, D21118, doi:10.1029/2011JD016610.

Yang, W., Hsieh, T.-L., and Vecchi, G. A.: Hurricane annual cycle controlled by both seeds and genesis probability, Proceedings of the National Academy of Sciences, 118, https://doi.org/10.1073/pnas.2108397118, 2021

Yeh, S.-W., Cai, W., Min, S.-K., McPhaden, M. J., Dommenget, D., Dewitte, B., … Kug, J.-S. (2018). ENSO atmospheric teleconnections and their response to greenhouse gas forcing. Reviews of Geophysics, 56, 185– 206. https://doi.org/10.1002/2017RG000568.

APPENDIX 2: ADDITIONAL NOTES FROM BREAKOUT GROUP SHEETS

Here little-changed comments from the breakout group sheets are provided for completeness:

TCWV

- Validation of surface values (e.g. specific humidity and relative humidity from stations and ships (2m)
- Understanding some of the processes leading to large scale anomalies - observed world/model world.
- 25% accuracy for 100 km monthly seems very large - 5% more useful?
- Stability requirements of daily 1 km seems very strict
- Model trends of order 1-2%/decade+-1%/decade at large scales probably require stability of order 0.2% per decade to be useful
- More work needs to be done to help users understand *how* best to compare model - satellite - in situ versions of reality.
- Would like to compare satellite with in-situ humidity (HadISDH) - but not clear if satellites can help with this?
- Applications of the high spatial resolution TCWV data over land might be more NWP than climate.
- Microwave: various sensors, assumption small scale similar observation time: simply average under the assumption of poor correlation. from there: different times, different sensor platforms, we assume no or very small correlation
- Come up with guideline in User Guide or *Dos and Don'ts* to apply CDRs
- Should we change to only clear-sky product for land and ocean surfaces? Theoretical product, since applied cloud masks would be different, a clear request was not formulated by the audience.
- Model output are only all-sky; would need to happen inside models
- Similar problem with sampling time: model are all-sky and all-time; CDR's are retrieval time (here around 10 am) and clear-sky over land

VRWV-UTLS

- Definition based on in-situ measurements: high vertical resolution requirements driven by dynamics (10 K = ~500m at 17km)
- Maximal sampling resolution in different domains (vertical, horizontal, temporal) always preferred (of course).
- "The" user requirements is an ill-defined concept. There are many applications each with their own requirements.
- But the most demanding application should not be the main driver of "the" final user requirements
- Target versus threshold requirements, it is sometimes discouraging for data providers to see ambitious requirements which cannot be met.
- Proposal: set requirements for future data records, not for existing/past sensors which are not designed tp meet these requirements..

VRWV-strato

- Definition of user requirements through CCI activities and GCOS initiatives
- OSSEs would be a better idea. Observations need to be able to detect inter-annual variability and long-term trends in VRWV, accounting for stratospheric methane increases

- Long-term trends in VRWV - is there evidence of changes in the BDC that affect tropical coldpoint temperatures and therefore stratospheric water vapor entry values?
- A count and classification of any short term events that are lost in an e.g. monthly dataset (E.g. sudden stratospheric warming, influences of overshooting convection).

APPENDIX 3: GLOSSARY

Term	Definition
ABC(t)	Atmosphere Biosphere Climate (teledetection)
ACE-FTS	Atmospheric Chemistry Experiment Fourier Transform Spectrometer
ACE-MAESTRO	Atmospheric Chemistry Experiment Measurements of Aerosol Extinction in the Stratosphere and Troposphere Retrieved by Occultation
AMSR-E	Advanced Microwave Scanning Radiometer for EOS
AMSU	Advanced Microwave Sounding Unit
ARA	Atmospheric Radiation Analysis
ARSA	Analyzed RadioSoundings Archive
AVHRR	Advanced Very High Resolution Receiver
BC	Brockmann Consult
CARIBIC	Civil Aircraft for the Regular Investigation of the atmosphere Based on an Instrument Container
CCI	Climate Change Initiative
CDO	Climate Data Operators
CDR	Climate Data Record
CDS	Copernicus Climate Data Store
CEDA	Centre for Environmental Data Analysis
CF	conventions for Climate and Forecast
CM SAF	EUMETSAT Satellite Application Facility on Climate Monitoring
CMAM	Canadian Middle Atmosphere Model
CMIP	Coupled Model intercomparison Project
CMUG	Climate Modelling User Group
CRG	Climate Research Group
DLR	Deutschen Zentrums für Luft- und Raumfahrt
DWD	Deutscher Wetterdienst (German MetService)
ECCC	Environment and Climate Change Canada
ECMWF	European Centre for Medium Range Forecast
ECV	Essential Climate Variable
EDA	ERA5 - reduced resolution ten member ensemble
EMiR	ERS/Envisat MWR Recalibration and Water Vapour Thematic Data Record Generation
Envisat	Environmental Satellite

Term	Definition
ERA5	ECMWF Re-Analysis 5
ERA-Interim	ECMWF Re-Analysis Interim
ESA	European Space Agency
ESGF	Earth System Grid Federation
EUMETSAT	European Organisation for the Exploitation of Meteorological Satellites
FOV	Field of View
FPH	Frost Point Hygrometer
GCOS	Global Climate Observing System
GEOS-5	Goddard Earth Observing System Model, Version 5
GMI	Global Precipitation Microwave Imager
GNSS	Global Navigation Satellite System
GOMOS	Global Ozone Monitoring by Occultation of Stars
GOZCARDS	Global OZone Chemistry And Related trace gas Data records for the Stratosphere
GPS	Global Positioning System
GRUAN	GCOS Reference Upper-Air Network
GUM	Guide to the Expression of Uncertainty in Measurement
HARMOZ	HARMonized dataset of Ozone profiles
HALOE	Halogen Occultation Experiment
HIRDLS	High Resolution Dynamics Limb Sounder
HOAPS	Hamburg Ocean Atmosphere Parameters and Fluxes from Satellite Data
IAGOS	In-service Aircraft for a Global Observing System
IASI	Infrared Atmospheric Sounder Interferometer
ILAS-II	Improved Limb Atmospheric Spectrometer-II
IMS	Infrared Microwave Sounding
IPSL-CM	Institut Pierre Simon Laplace - Climate Model
IR	Infrared
LMD	Laboratoire Météorologie Dynamique
LMS	lowermost stratosphere
LST	Land Surface Temperature
LWP	Vertically integrated liquid water
MERIS	Medium Resolution Imaging Spectrometer Instrument

Term	**Definition**
MERRA-2	Modern-Era Retrospective analysis for Research and Applications, Version 2
MHS	Microwave Humidity Sounder
MIPAS	Michelson Interferometer for Passive Atmospheric Sounding
MLS	Microwave Limb Sounder
MODIS	Moderate Resolution Imaging Spectrometer
MOZAIC	Measurement of OZone by Airbus In-service airCraft
MPI-M	Max-Planck Institute for Meteorology
MUDB	Match-up database
NASA	National Aeronautics and Space Administration
NCAR	National Center for Atmospheric Research
NCEO	National Centre for Earth Observation
NCEP	National Centers for Atmospheric Prediction
NDVI	Normalized Difference Vegetation Index
NIR	Near IR
NOAA	National Oceanic & Atmospheric Administration
NWP	Numerical Weather Prediction
OLCI	Ocean and Land Colour Instrument
PCs	Principle components
POAM	Polar Ozone and Aerosol Measurement
PSD	Product Specification Document
RAL	Rutherford Appleton Laboratory
RMS	Root mean square
RR	Reduced resolution
RTTOV	Radiative Transfer for TOVS
SAGE	Stratospheric Aerosol and Gas Experiment
SASBE	Site Atmospheric State Best Estimate
SCIAMACHY	Scanning Imaging Absorption Spectrometer for Atmospheric Cartography
SCISAT	Scientific Satellite
SE	Spectral Earth
SMILES	Solar wind Magnetosphere Ionosphere Link Explorer
SMR	Software Modification Report
SNR	Signal-to-noise ratio
SOFIE	Solar Occultation For Ice Experiment

Term	**Definition**
SPARC	Stratosphere-troposphere Processes And their Role in Climate
SPURT	Spurenstofftransport in der Tropopausenregion, trace gas transport in the tropopause region
SSM/I	Special Sensor Microwave Imager
SSMIS	Special Sensor Microwave Imager Sounder
SST	Sea Surface Temperature
SuomiNet	Global ground based GPS network (named after Verner Suomi)
SWOOSH	Stratospheric Water and OzOne Satellite Homogenized data set
TBD	To be determined
TCWV	Total Column Water Vapour
TMI	Tropical Rainfall Measuring Mission's Microwave Imager
TOA	Top Of Atmosphere
UKMO	United Kingdom Meteorological Office
UoL	University of Leicester
UoR	University of Reading
URD	User Requirements Document
UT	Upper Troposphere
UTLS	Upper Troposphere and Lower Stratosphere
UV	Ultraviolet
vis	Visible
VMR	Volume mixing ratio
VRes	Vertically resolved
WACCM	Whole Atmosphere Community Climate Model
WAVAS-I	Water Vapour Assessment
WAVAS-II	Water Vapour Assessment 2
WCRP	World Climate Research Programme
WGS	World Geodetic System 1984
WMO	World Meteorological Organization
WV	Water Vapour
WV_cci	Water Vapour climate change initiative

End of Document